Food Chemistry: X 40 (2026) 104800

Contents lists available at ScienceDirect

Food Chemistry: X

journal homepage: www.sciencedirect.com/journal/food-chemistry-x

Comparative metabolomics reveals the regulatory effects of different reducing sugar systems on non-volatile flavor compounds in whole-wheat lye bread

Jian Ma [a,1], Tuanjie Li [a,b,1], Rui Cao [a], Hui Zhao [a], Xuejie Li [a,c], Jing Lu [a], Lin Zhao [a,**], Jian Li [a,*]

[a] Key Laboratory of Green and Low-carbon Processing Technology for Plant-based Food of China National Light Industry Council, School of Food and Health, Beijing Technology and Business University, Beijing 100048, PR China
[b] Beijing Rijianeng Food Technology Co., Ltd., 100023, PR China
[c] Zhengzhou Tobacco Res Inst CNTC, Zhengzhou, Henan 450001, PR China

ARTICLE INFO

Keywords:
Reducing sugars
Maillard reaction
Electronic nose
Electronic tongue
Untargeted metabolomics

ABSTRACT

The Maillard reaction is a key pathway for flavor development in thermally processed foods. Whole-wheat lye breads were prepared with glucose alone (Glu) or glucose combined with fructose (GluFru), galactose (GluGal), or xylose (GluXyl). Binary sugar systems altered texture, color, sensory properties, and metabolite profiles. GluXyl produced softer bread, a stronger yellow-golden appearance, and enhanced umami and sweetness; its metabolite profile and higher melanoidin content were consistent with greater Maillard reaction progression. Electronic tongue (E-tongue) and electronic nose (E-nose) analyses indicated that GluGal exhibited more coordinated taste and aroma responses and the highest flavor harmony, accompanied by greater accumulation of Maillard-associated heterocyclic compounds, particularly alkylpyrazines and furan derivatives. Untargeted metabolomics revealed sugar-dependent differences in low-molecular-weight Maillard-associated reactions, with GluGal showing the largest number of differential metabolites ($n = 218$). Overall, xylose favored reaction progression, whereas galactose preferentially promoted flavor-related compound accumulation.

1. Introduction

Whole-wheat lye bread has emerged as a novel bakery product that integrates the nutritional advantages of whole grains with the characteristic sensory attributes of alkali-treated bread, attracting consumer interest (Sun et al., 2023). Compared with conventional pretzel bread made from refined wheat flour, whole-wheat pretzel bread uses whole-wheat flour as the main ingredient. Owing to the retention of bran and germ fractions, whole-wheat flour generally contains higher levels of dietary fiber, B vitamins, and minerals such as magnesium, iron, and zinc (Du et al., 2023; Wang et al., 2023; Wu et al., 2023). In addition, lye bread is generally formulated with little or no added sugar and fat. In whole-wheat formulations, the higher dietary fiber content and denser cereal matrix may slow starch digestion and potentially attenuate the postprandial glycemic response (Chekima et al., 2022; Lee, Roux, et al., 2024). These features make whole-wheat lye bread attractive to health-conscious consumers seeking cereal-based foods with improved nutritional profiles (Sun et al., 2023; Wang et al., 2023). However, compared with refined wheat bread, the incorporation of bran and germ also introduces a more complex flavor matrix (Wu et al., 2023). In particular, bran-associated notes, bitterness, and lipid oxidation-derived off-flavors may negatively affect the overall sensory quality and consumer acceptance of whole-wheat lye bread (Murayama et al., 2021; Palomino-Vasco et al., 2023). Therefore, improving the desirable baked aroma while minimizing undesirable flavor attributes remains a key challenge in the development of high-quality whole-wheat alkaline bakery products.

Recent advances in flavoromics and sensomics have highlighted that

* Corresponding author at: School of Food and Health, Beijing Technology and Business University, No. 11, Fucheng Road, Haidian District, Beijing 100048, PR China.
** Corresponding author.
E-mail addresses: 20251206@btbu.edu.cn (L. Zhao), lijian@th.btbu.edu.cn (J. Li).
[1] These authors contributed equally to this work.

https://doi.org/10.1016/j.fochx.2026.104800
Received 8 September 2026; Received in revised form 26 October 2026; Accepted 13 November 2026
Available online 13 November 2026
2590-1575/© 2026 The Authors. Published by Elsevier Ltd. This is an open access article under the CC BY license (http://creativecommons.org/licenses/by/4.0/).

flavor perception and acceptance are influenced by both volatile aroma compounds and non-volatile taste-active compounds, including products generated during thermal processing (Gu et al., 2025; Li, Qin, et al., 2025). In whole-wheat lye bread, these flavor-related compounds are generated through multiple, interconnected pathways, including yeast metabolism during dough proofing, lipid oxidation, caramelization, and Maillard-type reactions during baking (Du et al., 2023; Li, Qin, et al., 2025; Palomino-Vasco et al., 2023). Among these pathways, the Maillard reaction is particularly important because it contributes to desirable baked, caramel-like, nutty, and roasted aroma notes and is therefore an important target for flavor modulation in thermally processed foods (Bolchini et al., 2025; El Hosry et al., 2025; Shang et al., 2025; Yang et al., 2025).

Reducing sugar type plays a decisive role in regulating Maillard reaction pathways because different sugars differ in carbonyl reactivity, ring-opening equilibrium, degradation behavior, and their tendency to form specific reactive intermediates (El Hosry et al., 2025). Accordingly, selected reducing sugars may be used to modulate Maillard-derived flavor formation in thermally processed cereal foods. At the initial stage of the Maillard reaction, the carbonyl groups of reducing sugars react with free amino groups from amino acids, peptides, or proteins, with aldoses forming Amadori products and ketoses forming Heyns products (Chekima et al., 2022; Kaufmann et al., 2022). These early-stage products are generally not potent odorants; however, they serve as key chemical nodes that determine the subsequent formation of color- and flavor-active compounds (Yang et al., 2025). Their further enolization, dehydration, fragmentation, cyclization, and polymerization can lead to the generation of 5-hydroxymethylfurfural (5-HMF), furfural, Strecker aldehydes, pyrazines, pyrroles, furanones, melanoidins, and advanced glycation end-products (Bolchini et al., 2025; Shang et al., 2025). Therefore, different reducing sugar formulations may not simply alter the overall extent of the Maillard reaction, but may also redirect product formation toward distinct flavor-enhancing compounds and safety-related thermal reaction products (Bolchini et al., 2025; El Hosry et al., 2025).

To improve the flavor quality of whole-wheat lye bread without relying on exogenous flavor additives, this study modulated the reducing sugar systems in the formulation to promote the formation of Maillard reaction-derived flavor compounds. Specifically, whole-wheat lye breads were prepared using glucose (Glu) alone and three glucose-based binary reducing sugar systems, namely glucose-galactose (GluGal), glucose-xylose (GluXyl), and glucose-fructose (GluFru). In this study, selected Maillard reaction products, color parameters, textural properties, and sensory attributes were measured to systematically evaluate the effects of different reducing sugar systems on the quality of whole-wheat lye bread. Electronic nose (*E*-nose) and electronic tongue (E-tongue) analyses were further applied as instrumental sensory tools to characterize the overall aroma and taste fingerprints of breads prepared with different formulations (Mahanti et al., 2024; Zhang et al., 2025). Untargeted metabolomics was employed to profile non-volatile metabolites associated with Maillard reaction-mediated flavor modulation (Windarsih et al., 2022). This study aimed to clarify how different reducing sugar systems modulate flavor quality in whole-wheat lye bread and to provide a theoretical basis for improving flavor development in whole-grain bakery products.

2. Materials and methods

2.1. Materials

Whole-wheat flour was purchased from Shandong Tianqing Biotechnology Co., Ltd. (Shandong, China), and edible yeast was obtained from Angel Yeast Co., Ltd. (Hubei, China). Food-grade glucose, fructose, galactose, and xylose were purchased from Jiangsu Changjing Bioengineering Co., Ltd. (Jiangsu, China). Unless otherwise specified, all reagents used in this study were of food-grade quality.

2.2. Preparation of whole-wheat lye bread samples

Whole-wheat lye breads were prepared using the following basic formulation: 500 g of whole-wheat flour, 8 g of NaCl, 10 g of instant dry yeast, and 300 mL of water. Four dough formulations were prepared by adding 10 g of reducing sugars, including Glu, GluFru (1:1, w/w), GluXyl (1:1, w/w), and GluGal (1:1, w/w). For the binary sugar systems, the total sugar addition was maintained at 10 g, with 5 g of each sugar. All ingredients were mixed in a stand mixer at 24 °C until a homogeneous dough was formed. The dough was then rested at 24 °C for 20 min, divided into 40 g portions, rounded manually, and proofed at 4 °C for 30 min. Subsequently, the dough pieces were frozen at −18 °C for 40 min to stabilize their shape. The frozen dough pieces were immersed in 3.5% (w/v) food-grade sodium hydroxide solution for 30 s and then drained to remove excess alkali solution. Baking was performed in a preheated oven at upper and lower temperatures of 220 °C and 210 °C, respectively, for 15 min. After baking, the whole-wheat lye breads were cooled at room temperature for 60 min. Samples used for texture and other physical property measurements were analyzed without freezing. Separate portions intended for subsequent chemical and metabolomic analyses were immediately frozen in liquid nitrogen and stored at −80 °C until analysis.

2.3. Determination of Maillard reaction products

Acrylamide (AA) was determined by liquid chromatography-tandem mass spectrometry (LC-MS/MS) according to GB 5009.204-2025 and Cheng et al. (2021), with method performance evaluated in the whole-wheat bread matrix (Cheng et al., 2021). An AA reference standard (purity ≥99.9%; Shanghai Yuanye Bio-Technology Co., Ltd., Shanghai, China) was used. Analysis was performed using an Agilent 1260 LC system coupled to an Agilent 6475 triple-quadrupole mass spectrometer (Agilent Technologies, Santa Clara, CA, USA). Homogenized sample (1.00 g) was extracted with 10 mL of ultrapure water by shaking for 30 min and centrifuged at 4000×*g* for 10 min. The supernatant was defatted twice with 5 mL of n-hexane, followed by the addition of 10 mL of acetonitrile, 0.5 g of NaCl, and 4 g of anhydrous Na_2SO_4. After shaking for 5 min and centrifugation at 10,000×*g* for 5 min, a 2 mL aliquot was purified using a dispersive solid-phase extraction tube containing. The purified extract was centrifuged at 10,000×*g* for 5 min; 1 mL of the supernatant was evaporated to near dryness under nitrogen, reconstituted in 0.20 mL of ultrapure water, and filtered through a 0.22 μm membrane. Chromatographic separation was performed on an Agilent InfinityLab Poroshell 120 Aq-C_{18} column (2.1 mm × 100 mm, 2.7 μm, Agilent Technologies, Santa Clara, CA, USA) using 0.1% formic acid in water (A) and methanol (B) at 0.20 mL/min, with a 10 μL injection volume. The gradient was 95% A (0–3 min), 95–90% A (3–4 min), 90% A (4–6 min), 90–5% A (6–7 min), 5% A (7–8.5 min), 5–98% A (8.5–8.6 min), and 98% A (8.6–10 min). AA was detected in positive electrospray ionization mode using multiple-reaction monitoring, with *m/z* 72.0 → 55.0 as the quantifier transition. The source conditions were a nozzle voltage of 2000 V, source-heater temperature of 150 °C, gas temperature of 330 °C, nebulizer pressure of 90 psi, and collision-gas flow of 0.15 mL/min. External calibration was performed over 10–1000 μg/L, yielding ($y = 6785.22 * x + 8404.08$) ($R^2 = 0.9972$), where (x) was AA concentration (μg/L) and (y) was peak area. Matrix-spike recoveries at 100, 500, and 1000 μg/kg were 93.79–102.64%, with relative standard deviations (RSDs) of 7.23–10.19%. The solution-level limit of detection (LOD) and (limit of quantification) LOQ were 3.23 and 10.17 μg/L, respectively, based on signal-to-noise ratios of 3 and 10. Three independently prepared sample extracts were analyzed per treatment, and results were expressed as μg/kg bread.

The detection method for 5-HMF was adapted from Jozinović et al. (2019), with minor modifications (Jozinović et al., 2019). A 5-HMF reference standard (purity ≥98.0%; Shanghai Yuanye Bio-Technology Co., Ltd., Shanghai, China) was used. Sample preparation was

performed as described above for AA. Chromatographic separation was achieved on an InfinityLab Poroshell 120 Aq-C_{18} column using 0.1% formic acid in water (A) and methanol (B) at a ratio of 95:5 (v/v) under isocratic conditions. The flow rate was 0.25 mL/min, the column temperature was 35 °C, and the injection volume was 2 μL. Detection was performed using an Agilent 6475 triple-quadrupole mass spectrometer equipped with a Jet Stream electrospray ionization source in positive-ion multiple-reaction monitoring (MRM) mode, with *m/z* 127.0 → 109.0 as the quantifier transition. The ion-source conditions were identical to those described for AA. External calibration over 100–1000 μg/L yielded (y = 3654.85 * x + 2447.30) (R^2 = 0.9975), where x was the 5-HMF concentration (μg/L) and y was the corresponding peak area. Matrix-spike recoveries at 1, 5, and 10 mg/kg ranged from 98.05% to 106.31%, with RSDs of 3.38–9.52%. The solution-level LOD and LOQ, determined at signal-to-noise ratios of 3 and 10, were 25.45 and 80.73 μg/L, respectively. Three independently prepared sample extracts were analyzed for each treatment, and results were expressed as mg/kg bread.

Nε-(carboxymethyl)lysine (CML) and Nε-(carboxyethyl)lysine (CEL) were quantified by LC-MS/MS. following Cheng et al. (2021), with minor modifications (Cheng et al., 2021). Reference standards of CML (purity ≥97.0%) and CEL (purity ≥95.0%) were obtained from Shanghai Yuanye Bio-Technology Co., Ltd. (Shanghai, China). For determination of total CML and CEL, approximately 100 mg of pulverized sample was reduced with 5.0 mL of $NaBH_4$ solution (0.2 M $NaBH_4$ in 0.1 M NaOH) for 4 h at room temperature to minimize artefactual formation of advanced glycation products during hydrolysis. Excess $NaBH_4$ was decomposed with 2 mL of formic acid, after which 5 mL of 6 M HCl was added. Samples were hydrolyzed under nitrogen at 110 °C for 22 h, evaporated to dryness under nitrogen, reconstituted in 1 mL of 0.1% formic acid, and purified using a solid-phase extraction cartridge. The purified extracts were filtered through 0.22 μm aqueous membranes before LC-MS/MS analysis. Chromatographic separation was performed on an InfinityLab Poroshell 120 Aq-C_{18} column using 0.1% formic acid in water (A) and methanol (B) at 0.25 mL/min. The gradient was 98% A (0–1 min), 98–95% A (1–4 min), 95–90% A (4–6 min), and 90–98% A (6–9 min), with a total run time of 9 min. The column temperature was 35 °C and the injection volume was 2 μL. Detection was performed using an Agilent 6475 triple-quadrupole mass spectrometer equipped with a Jet Stream electrospray ionization source in positive-ion dynamic MRM mode. The monitored transitions were *m/z* 205.1 → 84.1 (quantifier) and 205.1 → 130.0 (qualifier) for CML, and *m/z* 219.1 → 84.1 (quantifier) and 219.1 → 130.1 (qualifier) for CEL. The source conditions were a nozzle voltage of 800 V, source heater temperature of 120 °C, gas temperature of 350 °C, nebulizer pressure of 100 psi, and collision gas flow of 0.17 mL/min. Data acquisition and quantitative processing were performed using Agilent MassHunter Workstation software (version 12.0, Agilent Technologies, Santa Clara, CA, USA). Because the analysis was conducted using predefined targeted dynamic MRM transitions rather than full-scan acquisition or spectral-library matching, no full-scan mass range or spectral-matching threshold was applied. External calibration over 10–500 μg/L yielded (y = 6757.56 * x + 3639.23) (R^2 = 0.9989) for CML and (y = 877.63 * x + 381.22) (R^2 = 0.9993) for CEL, where (x) represents analyte concentration (μg/L) and (y) the corresponding peak area. Matrix-spike recoveries at 10, 30, and 50 mg/kg were 98.68–105.94% for CML (RSD, 6.26–9.77%) and 96.11–102.88% for CEL (RSD, 4.67–8.44%). The solution-level LOD and LOQ were 4.86 and 9.77 μg/L for CML and 2.76 and 7.17 μg/L for CEL, respectively. Three independently prepared sample extracts were analyzed for each treatment, and results were expressed as mg/kg bread.

Soluble melanoidin-associated browning products were semi-quantified by UV–visible spectrophotometry using glucose–serine Maillard reaction products as a surrogate standard (Yang et al., 2019). Glucose and serine (0.05 mol each) were dissolved in ultrapure water, freeze-dried, and heated at 90 °C for 1 h. After cooling, known amounts of the resulting brown products were dispersed in ultrapure water to prepare standards of 0.1–5.0 mg/mL, and absorbance was measured at 420 nm. Pulverized samples were extracted with ultrapure water at a solid-to-liquid ratio of 1:50 (*w/v*), vortex-mixed for 10 min, and sonicated in an ice-water bath for 30 min at 250 W and 100 kHz. After centrifugation at 10000 ×*g* for 12 min at 4 °C, the supernatants were filtered through 0.45 μm aqueous membranes and measured at 420 nm. External calibration yielded (y = 1.053 * x + 0.063) (R^2 = 0.9933), where (x) is the nominal concentration of the glucose–serine Maillard reaction products (mg/mL) and (y) is the absorbance at 420 nm. Results were expressed as glucose-serine model-melanoidin equivalents (g/100 g sample) and interpreted as semi-quantitative equivalents rather than absolute melanoidin concentrations.

2.4. Determination of color difference

The L* (lightness), a* (redness/greenness), and b* (yellowness/blueness) values were measured using a portable colorimeter (CR-20, Konica Minolta, Japan). The total color difference (ΔE*) was calculated using the following formula:

$$\Delta E^* = \sqrt{(L^* - L_0{}^*)^2 + (a^* - a_0{}^*)^2 + (b^* - b_0{}^*)^2}$$

where L_0*, a_0*, and b_0* are the color parameters of the control sample.

2.5. Determination of texture properties and texturized

The hardness, cohesiveness, gumminess, resilience, springiness, and chewiness of the samples were determined using a texture analyzer (TMS-Touch, Food Technology Corporation, Virginia, USA) in texture profile analysis (TPA) mode. The TPA parameters were set as follows: test speed, 1.0 mm/s; compression ratio, 50%; trigger force, 1 N; and return distance, 15 mm (Hernandez-Aguilar et al., 2021). For each analysis, samples were cut into uniform pieces measuring 50 mm × 50 mm × 10 mm. Nine replicate measurements were performed for each sample, and the average value was calculated after excluding outliers.

2.6. Sensory evaluation

The sensory evaluation was approved by the Ethics Committee of Beijing Technology and Business University (No.2024140, Beijing, China). All sensory experiments were performed in a standard sensory laboratory according to ISO 8589-2007. Fifteen evaluators, eight males and seven females each with extensive training in sensory evaluation, were recruited from Beijing Technology and Business University. Based on previous studies on bread flavor and Maillard reaction-derived sensory characteristics, a sensory descriptor list was established through panel discussion and consensus. The selected attributes included roasted aroma, caramel aroma, sweet aroma, burnt aroma, sweetness, bitterness, aftertaste intensity, color intensity, and flavor harmony (Bolchini et al., 2025; El Hosry et al., 2025; Mahanti et al., 2024; Zhang et al., 2025). During the evaluation, these sensory attributes were assessed using 9-point scales with attribute-specific anchors, as detailed in Table S1. Scores of 1–3, 4–6, and 7–9 represented weak/low, moderate, and strong levels, respectively. Overall liking was assessed separately using a 9-point hedonic scale, anchored at 1 = “dislike extremely”, 5 = “neither like nor dislike”, and 9 = “like extremely”.

2.7. E-nose analysis

The operating conditions of the E-nose were based on the method reported by (Zhang et al., 2025), with slight modifications. Briefly, 5 g of each sample was accurately weighed and transferred into a 25 mL amber headspace vial. The vial was immediately sealed with a PTFE/silicone septum to prevent the loss of volatile compounds. After equilibration at 50 °C for 40 min, the headspace gas was analyzed using an E-nose system (PEN3, Honglin Scientific Instrument Co., Ltd., Hunan, China). The system was equipped with an array of ten metal oxide sensors, and the

sensitivity characteristics of each sensor are listed in Table S2. Before each measurement, the sensor array was purged with clean air filtered through activated carbon to stabilize the baseline response and minimize carryover effects from previous analyses. Subsequently, the headspace gas was introduced into the sensor chamber through a sampling needle at a flow rate of 300 mL/min. The total acquisition time was set to 100 s. After stabilization of the sensor response curves, the response values recorded at 60 s were extracted as representative data for subsequent statistical analysis.

2.8. E-tongue analysis

The taste profile of each sample was analyzed using a Taste-Sensing System SA 402B E-tongue (Intelligent Sensor Technology Co., Ltd., Atsugi, Japan). Six taste sensors, namely AAE, CT0, CA0, C00, AE1, and GL1, together with two reference electrodes, were used for the analysis. Before measurement, all sensors were conditioned in the reference solution for 24 h to ensure signal stability. For sample preparation, 5 g of each sample was accurately weighed, mixed with 100 mL of distilled water, and subjected to sonication for 3 h to extract water-soluble taste-active compounds. The extract was then filtered, and the filtrate was collected for subsequent E-tongue analysis. Taste intensity values were calculated by multiplying the sensor outputs by the corresponding coefficients according to the Weber–Fechner law, thereby converting sensor responses into perceived taste intensities (Zhu et al., 2022).

2.9. Untargeted metabolomics analysis

For metabolite extraction, 25 mg of each sample was accurately weighed into a microcentrifuge tube, followed by the addition of two homogenization beads and 500 μL of extraction solvent consisting of methanol/acetonitrile/water at a ratio of 2:2:1 (v/v/v). The extraction solvent contained isotope-labelled internal standards. The mixture was vortexed for 30 s, homogenized at 35 Hz for 4 min, and then sonicated in an ice-water bath for 5 min. This homogenization–sonication cycle was repeated three times. The samples were then kept at −40 °C for 1 h to facilitate protein precipitation and metabolite extraction. Subsequently, 300 μL of the extract was transferred to a 96-well filter plate. The assembled 96-well filter plate and collection plate were placed in a positive-pressure manifold and slowly pressurized to 6 psi for 3 min. The filtrate was collected and subjected to LC-MS analysis. Equal aliquots of filtrate from all samples were pooled to prepare quality control (QC) samples, which were analyzed throughout the sequence to monitor instrumental stability.

For polar metabolite analysis, chromatographic separation was performed using a Vanquish ultra-high-performance liquid chromatography system (Thermo Fisher Scientific, USA) equipped with a Waters ACQUITY UPLC BEH Amide column (2.1 mm × 50 mm, 1.7 μm). Mobile phase A consisted of water containing 25 mmol/L ammonium acetate and 25 mmol/L ammonia, whereas mobile phase B was acetonitrile. The autosampler temperature was maintained at 4 °C, and the injection volume was 2 μL.

For non-polar metabolite analysis, chromatographic separation was conducted using the same Vanquish UHPLC system equipped with a Phenomenex Kinetex C18 column (2.1 mm × 50 mm, 2.6 μm). Mobile phase A was water containing 0.01% acetic acid, and mobile phase B consisted of isopropanol/acetonitrile at a ratio of 1:1 (v/v). The autosampler temperature was maintained at 4 °C, and the injection volume was 2 μL. Mass spectrometric data were acquired using an Orbitrap Exploris 120 mass spectrometer controlled by Xcalibur software (version 4.4, Thermo Fisher Scientific). The main MS parameters were set as follows: sheath gas flow rate, 50 Arb; auxiliary gas flow rate, 15 Arb; capillary temperature, 320 °C; full MS resolution, 60000; MS/MS resolution, 15000; stepped normalized collision energy, 20/30/40; spray voltage, 3.8 kV in positive ion mode and −3.4 kV in negative ion mode. The raw data were converted to mzXML format using ProteoWizard software (version 3.0.24054). Subsequent data processing and metabolite annotation were performed using R software (version 4.5.1; R Foundation for Statistical Computing, Vienna, Austria), with reference to the BiotreeDB database (version 4.0).

2.10. Statistical analysis

The figures were plotted using Origin 2021 software (Chicago, IL, USA). Analysis of variance (ANOVA) was conducted by IBM SPSS version 22.0 (Armonk, New York, NY, USA). As $p < 0.05$, it was considered to significant differences. MetaboAnalyst6.0 (https://www.metaboanalyst.ca/, McGill University, Montreal, Canada) was used for non-targeted metabolomics data analysis. Variable importance in projection (VIP)values were derived from the orthogonal partial least squares discriminant analysis (OPLS-DA) model, and univariate statistical significance was evaluated using p values. To correct for multiple comparisons and minimize false-positive findings, p values were adjusted using the FDR method. Metabolites with VIP > 1.0, fold change (FC) > 2 or < 0.5, and $p < 0.05$ were considered candidate differential metabolites. Unless otherwise specified, all experiments were performed in triplicate, and data were expressed as the mean ± standard deviation (SD).

3. Results and discussion

3.1. Sensory analysis

As shown in Fig. 1(a-d), the sensory profiles of whole-wheat lye breads were significantly affected by the type of reducing sugar system incorporated into the formulation ($p < 0.05$), indicating that sugar composition played an important role in modulating flavor development during alkaline baking. Compared with the Glu sample, the binary reducing sugar systems generally exhibited improved sensory performance, particularly in roasted aroma, caramel aroma, sweetness perception, and overall flavor preference. This phenomenon may be attributed to the different reactivity and degradation pathways of reducing sugars during the Maillard reaction, which can generate distinct intermediate compounds and final flavor-active products (El Hosry et al., 2025).

Theng et al. (2024) reported that different reducing sugars generate distinct volatile compounds, including furans, Strecker aldehydes, and pyrazines, during the Maillard reaction (Theng et al., 2024). In this study, GluFru and GluGal breads exhibited the highest roasted aroma and caramel aroma intensities, followed by GluXyl, whereas the Glu bread showed the lowest scores. The enhancement of roasted aroma in binary sugar formulations may be attributed to the increased diversity of Maillard reaction intermediates resulting from differences in sugar structure and reactivity. Different reducing sugars can redirect Maillard pathways toward specific flavor compounds depending on their carbonyl reactivity and degradation behavior (Pham et al., 2025). Among the formulations, GluGal exhibited the highest flavor harmony and relatively favorable overall liking. For taste-related attributes, the differences in sweetness scores suggested that perceived sweetness was not solely determined by residual sugar concentration but was also influenced by interactions between remaining sugars, Maillard-derived compounds, and bitter flavor components. During baking, reducing sugars are partially consumed through Maillard reactions and caramelization, resulting in complex changes in taste perception. However, the enhancement of Maillard-derived aroma was also accompanied by increased bitterness-related attributes in some formulations. Both the GluXyl and GluFru systems exhibited relatively high scores for burnt/bitter notes and overall bitterness.

These results suggest that the excessive formation of thermal reaction products may negatively affect sensory acceptance. Previous flavoromics studies on whole-wheat bread have shown that non-volatile compounds, including lipid oxidation products and bitter compounds,

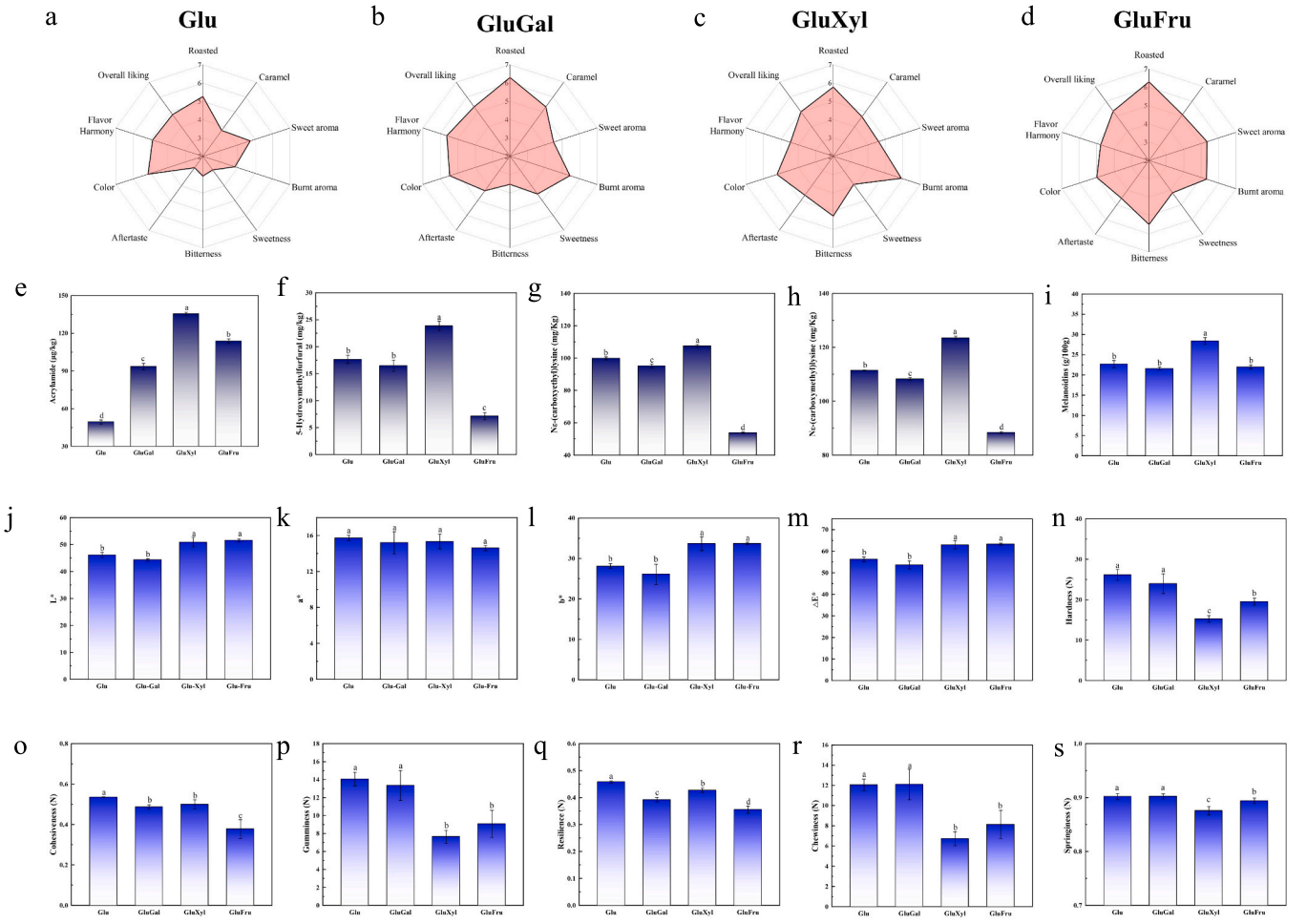

Fig. 1. Sensory evaluation and physicochemical characteristics of whole-wheat lye breads prepared with Glu, GluGal, GluXyl, and GluFru formulations. (a, b, c, d): Sensory evaluation results for Glu, GluGal, GluXyl, and GluFru. (e): Acrylamide. (f): 5-Hydroxymethylfurfural. (g): Nε-(carboxyethyl)lysine. (h): Nε-(carboxymethyl) lysine. (i): Model-melanoidin. (j): L*. (k): a*. (l): b*. (m): ΔE*. (n): Hardness. (o): Cohesiveness. (p): Gumminess. (q): Resilience. (r): Chewiness. (s): Springiness. Lowercase letters mark statistically significant differences with one-way ANOVA test of significance among sample ($p < 0.05$).

can significantly reduce consumer liking (Cong et al., 2021). Non-targeted LC-MS analysis has identified various non-volatile compounds (such as trihydroxy fatty acids and phospholipid derivatives) as key contributors to the perception of bitterness in whole-wheat bread (Pham et al., 2025). Therefore, improving flavor quality requires balancing the generation of desirable roasted aroma compounds and the suppression of undesirable bitter or burnt characteristics.

Among the formulations, GluGal exhibited the highest flavor harmony and relatively favorable overall liking, suggesting that combining glucose with another reducing sugar could improve the overall sensory acceptability of whole-wheat lye bread, although excessive Maillard reactions in dual-sugar systems may also have contributed to the formation of undesirable flavors.

3.2. Analysis of Maillard reaction product contents

The formation of Maillard reaction markers in whole-wheat lye breads was strongly influenced by the type of reducing sugar system incorporated into the formulation (Fig. 1(e-i)). AA, 5-HMF, CEL, CML, and model-melanoidin exhibited different formation patterns among the four formulations, indicating that reducing sugar composition not only affected the overall extent of the Maillard reaction but also redirected reaction pathways toward different intermediate and final products (Bolchini et al., 2025; Yang et al., 2025).

Among the four formulations, GluXyl showed the highest levels of AA (135.648 ± 1.033 μg/kg), 5-HMF (23.881 ± 0.887 mg/kg), CEL (107.575 ± 0.912 mg/kg), and CML (123.489 ± 0.684 mg/kg), suggesting that the GluXyl system promoted a stronger formation of both early and advanced Maillard reaction products. Unlike hexoses (glucose, galactose, fructose), xylose has a shorter carbon chain, resulting in a lower activation energy for the initial condensation reaction with amino groups (Bolchini et al., 2025; El Hosry et al., 2025). This favored the formation of early-stage Amadori products, which could subsequently degrade through enolization, dehydration, and fragmentation to generate deoxyosones and reactive α-dicarbonyl compounds. These intermediates participated in several downstream pathways, 3-deoxyglucosone and related hexose-derived intermediates could contribute to 5-HMF formation, while advanced glycation end products such as CML and CEL could arise through Amadori-product degradation and reactions of lysine with reactive dicarbonyls such as glyoxal and methylglyoxal. In contrast, AA was formed mainly through a distinct asparagine-carbonyl pathway involving Schiff-base formation, decarboxylation, and subsequent degradation during high-temperature processing. (Yang et al., 2025). Therefore, the elevated levels of CML and CEL in GluXyl bread may be associated with the increased formation of reactive dicarbonyl intermediates derived from xylose degradation. Melanoidins are high-molecular-weight brown polymers generated during the advanced stages of the Maillard reaction and are closely

related to crust browning, roasted aroma formation, and antioxidant activity (El Hosry et al., 2025). The higher melanoidin content observed in GluXyl bread corresponded well with its stronger burnt/bitter sensory perception, indicating that extensive Maillard reaction progression may favor the accumulation of polymerized brown compounds associated with darker color and more intense roasted or burnt notes.

AA is mainly generated through the reaction between reducing sugars and free asparagine during thermal processing, particularly under low-moisture and high-temperature baking conditions (El Hosry et al., 2025). In this study, GluXyl exhibited the highest AA concentration, whereas GluFru showed the second level (113.773 ± 1.882 μg/kg). This difference suggests that fructose-containing systems may follow different carbonyl transformation pathways during alkaline baking (Windarsih et al., 2022). Although fructose is highly reactive in Maillard chemistry, its degradation may favor alternative pathways leading to other furan derivatives or flavor-active compounds rather than AA accumulation under specific processing conditions.

5-HMF is primarily generated through sugar dehydration reactions, particularly from hexose-derived intermediates formed during advanced Maillard reaction and caramelization (Gu et al., 2025). The relatively low 5-HMF level in GluFru bread suggests that fructose may have undergone alternative degradation routes or interacted differently with amino compounds during alkaline baking. In contrast, the higher 5-HMF accumulation in GluXyl indicates that the pentose-derived pathway may facilitate dehydration reactions and the formation of furan compounds. These results highlight that reducing sugar type determines not only reaction intensity but also the distribution of specific thermal degradation products.

Overall, these results demonstrate that different reducing sugar systems exert distinct regulatory effects on Maillard reaction pathways in whole-wheat lye bread. The GluXyl system exhibited a greater extent of Maillard reaction, as evidenced by the increased formation of AA, 5-HMF, CML, CEL, and model melanoidins, together with markedly enhanced roasted and burnt sensory attributes. In contrast, the GluGal formulation showed a Maillard reaction extent comparable to that of the Glu formulation while achieving a greater improvement in the overall flavor quality of the final product.

3.3. Texture and color difference analysis

In bakery products, crust color is generally governed by non-enzymatic browning reactions, mainly the Maillard reaction and caramelization, which are affected by sugar type, amino compound availability, pH, water activity, and thermal history (Jost et al., 2021; Shakoor et al., 2022). As shown in Fig. 1(j-m), the color characteristics of whole-wheat lye breads were markedly influenced by the reducing sugar system. The GluFru and GluXyl sample showed the highest L* value ($p < 0.05$), followed by Glu (46.16 ± 0.98), and GluGal (44.37 ± 0.39). Since L* represents lightness, these results indicate that the GluFru and GluXyl formulations produced a lighter and brighter crust appearance, whereas GluGal resulted in a darker visual tone.

The a* values showed relatively small variation among formulations, ranging from 14.63 ± 0.28 in GluFru to 15.75 ± 0.29 in Glu. This suggests that the red-green component was not the main factor responsible for the overall color differentiation among the four breads. In contrast, the b* values differed more clearly. In contrast, the b* values differed more clearly. GluFru and GluXyl exhibited similar b* values (33.72 ± 0.34 and 33.70 ± 1.72, respectively; $p > 0.05$ between the two groups), and both were significantly higher than those of Glu and GluGal ($p < 0.05$), indicating a stronger yellow-golden color contribution in the GluFru and GluXyl samples. These results suggested that binary sugar systems did not merely darken the bread surface but shifted the crust color toward distinct brown-yellow tonalities (Giovanelli & Cappa, 2021).

The ΔE* values followed the order GluFru and GluXyl > Glu and GluGal ($p < 0.05$). These differences were mainly attributable to their higher L* and b* values rather than to a pronounced increase in a*. As a ketose, fructose can participate in the Maillard reaction through Heyns-type intermediates and can also undergo dehydration and caramelization during baking (Lee, Roux, et al., 2024; Pham et al., 2025). GluFru may favor the formation of yellow-golden chromophores through fructose dehydration and caramelization-related pathways. In contrast, xylose, as a pentose, generally exhibits higher Maillard reactivity than hexoses and is more likely to promote the formation of reactive carbonyl intermediates and downstream browning products (Yang et al., 2025). GluXyl may promote Maillard-derived browning through the higher reactivity of xylose. Therefore, the elevated L*, b*, and ΔE* values observed for these two formulations suggested that reducing-sugar composition reshaped crust color formation by modulating both Maillard reaction progression and chromophore formation derived from sugar degradation (El Hosry et al., 2025).

As shown in Fig. 1(n-s), the reducing sugar system significantly affected the textural properties of whole-wheat lye breads. The Glu showed the highest hardness (26.155 ± 1.349 N) ($p < 0.05$), followed by the GluFru group, while the GluXyl group showed the lowest value (15.297 ± 0.804 N) ($p < 0.05$). This result indicated that, compared with glucose alone, the GluXyl and GluFru formulations produced a softer bread matrix. Similar trends were observed for gumminess and chewiness. The Glu showed the highest gumminess and chewiness values (14.076 ± 0.753 N, and 12.056 ± 0.582 N, respectively), whereas GluXyl showed the lowest values (7.664 ± 0.719 N, and 6.732 ± 0.692 N, respectively) ($p < 0.05$). Since gumminess and chewiness are mainly derived from hardness, cohesiveness, and springiness, these results suggest that the GluXyl system effectively reduced the resistance of whole-wheat lye bread to compression and mastication.

Cohesiveness and resilience further reflected differences in internal structural integrity. Glu showed the highest cohesiveness (0.536 ± 0.001) and resilience (0.459 ± 0.004) ($p < 0.05$), indicating a more compact and recoverable matrix. In contrast, GluFru exhibited the lowest cohesiveness (0.379 ± 0.046) and resilience (0.356 ± 0.013) ($p < 0.05$), suggesting weaker internal bonding. GluXyl maintained moderate cohesiveness (0.500 ± 0.023) and resilience (0.428 ± 0.008) despite its lowest hardness, implying that this formulation softened the product without causing excessive structural collapse. Springiness changed only slightly among samples, ranging from 0.876 ± 0.008 for GluXyl to 0.903 ± 0.005 for GluGal. These observations indicated that reducing-sugar type primarily influenced firmness and chewing resistance rather than elastic recovery. These differences may be related to the combined effects of sugar composition and processing conditions. Different reducing sugars can influence yeast fermentation, osmotic pressure, water distribution, starch gelatinization, and gluten network development, thereby modifying bread firmness and matrix stability (Sawettanun et al., 2023; Xiao et al., 2025). Therefore, the lower hardness, gumminess, and chewiness observed in GluXyl may be associated with sugar-dependent changes in dough structure formation and moisture redistribution during fermentation, alkaline treatment, and baking.

Overall, GluXyl system exhibited the most pronounced Maillard reaction characteristics while maintaining favorable textural and color properties, whereas GluGal showed a comparatively moderate extent of Maillard reaction but relatively favorable flavor attributes.

3.4. E-nose analysis results

3.4.1. Radar plot analysis

The E-nose radar plot showed clear differences in the overall volatile fingerprints of whole-wheat lye breads prepared with different reducing sugar systems (Fig. 2). The discrimination among formulations was mainly driven by the high-response sensors W1W, W2S, W5S, and W1S, whereas W1C, W3C, and W5C showed relatively low responses, with no significant differences among the samples ($p > 0.05$).

Among the four formulations, GluXyl exhibited the strongest

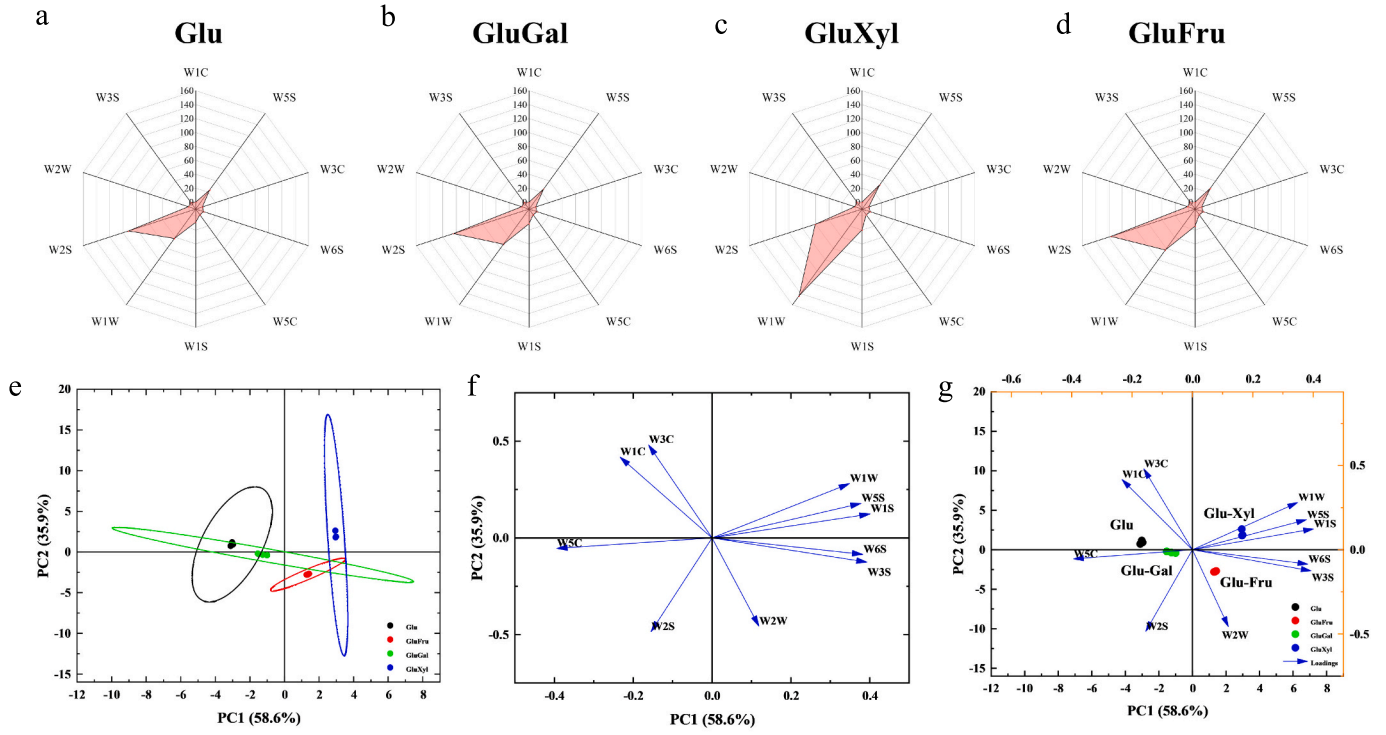

Fig. 2. E-nose detection results for Glu, GluGal, GluXyl, and GluFru. (a-d): Radar Chart for Glu, GluGal, GluXyl, and GluFru. (e): PCA scores plot. (f): PCA loadings plot. (g): Combined plot of PCA analysis results.

response on W1W (144.54 ± 0.60) ($p < 0.05$), which was much higher than GluFru (62.55 ± 0.51), GluGal (52.53 ± 0.29), and Glu (42.53 ± 0.44). GluXyl also showed the highest responses on W5S (32.95 ± 0.95) and W1S (19.90 ± 0.22) ($p < 0.05$). These results indicate that the GluXyl formulation produced a stronger and distinct volatile sensor-response profile. This difference may be associated with the relatively high Maillard reactivity of xylose as a pentose, which can facilitate the formation of reactive carbonyl intermediates and subsequent volatile reaction products during alkaline baking (Giovanelli & Cappa, 2021). Under high-temperature, low-moisture, and alkaline conditions, xylose may participate more readily in Maillard reactions, thereby contributing to the overall differences in volatile profiles among the formulations (Cong et al., 2021; Ding et al., 2024; Lee, Roux, et al., 2024). However, because electronic-nose sensors provide non-specific, cross-sensitive responses, the identities and relative abundances of individual volatile compounds cannot be determined without complementary chromatographic analysis such as gas chromatography–mass spectrometry.

Gancarz et al. (2021) also reported that fermentation and thermal processing can markedly modify the volatile-compound fingerprints of bread and cereal-based products (Gancarz et al., 2021). In contrast, GluFru showed the strongest response on W2S (117.32 ± 0.41) ($p < 0.05$), followed by GluGal, Glu, and GluXyl, corresponding to sweet, fruity, and floral volatiles. The high W2S response in GluFru may indicate a stronger contribution of oxygen-containing volatiles, such as alcohols, aldehydes, ketones, or furan-related compounds. These volatiles were likely derived from fructose degradation and caramelization-related reactions, resulting in a volatile profile distinct from that of the GluXyl formulation (Li, Qin, et al., 2025; Sawettanun et al., 2023). GluGal generally showed intermediate *E*-nose responses. This suggested that the GluGal system produced a more moderate volatile profile than GluXyl and GluFru. Overall, the role of binary reducing sugar systems was not limited to enhancing aroma intensity; rather, they reshaped the compositional balance of volatile compounds in whole-wheat lye bread.

3.4.2. *Principal component analysis (PCA) of E-nose results*

PCA enables dimensionality reduction and interpretation of high-dimensional complex omics and sensory datasets, serving as a widely used multivariate statistical approach to discriminate sample variations and identify key variables (Wu et al., 2023; Zhang et al., 2025). The PCA plots based on E-nose responses showed clear separation among whole-wheat lye breads prepared with different reducing sugar systems, indicating that sugar composition markedly reshaped the overall volatile fingerprints of the products (Fig. 2(e-g)). Based on the standardized sensor responses, PC1 and PC2 explained 58.6% and 35.9% of the total variance, respectively, accounting for 94.5% of the overall information. This high cumulative variance suggests that the first two principal components were sufficient to describe the major aroma differences among the four formulations.

The PCA score plot showed that GluXyl was clearly separated from the other formulations, mainly along the direction associated with W1W, W5S, W1S, W6S, and W3S in the loading plot (Fig. 2f). This separation was consistent with the radar plot results, in which GluXyl exhibited the highest responses for W1W, W5S, and W1S. These sensors are broadly responsive to sulfur-containing compounds, nitrogen oxides, methane-related compounds, and other highly reactive volatile components. The strong response of GluXyl may be associated with the higher Maillard reactivity of xylose during alkaline baking (Shakoor et al., 2022). In contrast, GluFru was positioned closer to the positive direction of PC2, which was mainly associated with W2S and W2W. And the W2S sensor is commonly associated with oxygen-containing volatiles, including alcohols, aldehydes, ketones, and related compounds. Therefore, the GluFru formulation may have favored the formation or release of oxygenated volatiles derived from fructose degradation, caramelization, and fermentation-related pathways (Lee, Roux, et al., 2024; Wu et al., 2023; Xiao et al., 2025). The GluGal samples occupied an intermediate region in the PCA space. This indicated that the GluGal produced a less intense but more balanced volatile fingerprint than GluXyl and GluFru. By comparison, Glu showed relatively lower

responses for the main discriminating sensors, suggesting that glucose alone generated a weaker overall aroma fingerprint under the same processing conditions.

The PCA results indicated that the differences in volatile fingerprints were mainly driven by formulation-dependent effects rather than processing-induced variation. GluXyl was characterized by stronger responses from sensors associated with Maillard-derived volatile fingerprints, whereas GluFru was more closely related to oxygenated volatile signals. These findings suggest that binary reducing sugar systems did not simply increase aroma intensity but reshaped the volatile composition of whole-wheat lye bread into distinct aroma fingerprints.

3.5. E-tongue analysis results

3.5.1. Radar plot analysis

The E-tongue system enables objective characterization of taste-related information in complex food matrices and reduces the subjective bias associated with human sensory evaluation, making it an important instrumental tool for comparing taste differences among samples (Zhu et al., 2022). The E-tongue results revealed that the reducing sugar system reshaped the overall taste profiles of whole-wheat lye breads, particularly in sourness, bitterness, astringency, umami, saltiness, and sweetness (Fig. 3(a-d)). It should be noted that E-tongue values represent relative sensor outputs rather than direct concentrations of taste compounds.

Among the four formulations, GluXyl showed the lowest sourness response (-51.953 ± 0.264) ($p < 0.05$), whereas Glu showed the highest value (-45.112 ± 0.354) ($p < 0.05$). This trend indicated that binary reducing sugar systems, especially GluXyl, reduced the relative sourness response compared with glucose alone. Since all breads were produced under the same fermentation, alkaline dipping, and baking conditions, this difference was more likely caused by formulation-dependent changes in sugar utilization, organic acid balance, and buffering effects during dough fermentation and baking (Dos Santos Rocha et al., 2023; Palomino-Vasco et al., 2023). In fermented cereal systems, organic acids, amino acids, soluble peptides, and sugars jointly determine electronic tongue responses. Similarly, Li, Yuan, et al. (2025) reported that changes in formulation or fermentation strategy can alter taste-related signals associated with sourness, bitterness, and umami in steamed buns (Li, Yuan, et al., 2025).

Bitterness showed a different response pattern. The Glu sample had the highest bitterness value (9.111 ± 0.135) ($p < 0.05$), whereas GluFru and GluGal showed lower responses ($p < 0.05$). This result suggested that the binary reducing sugar systems did not necessarily increase bitterness, even though they may have participated more actively in Maillard reaction and browning processes (Bolchini et al., 2025). Astringency and aftertaste responses further supported the role of binary reducing sugar systems in modulating taste quality. GluXyl exhibited the lowest astringency response (-1.631 ± 0.027), followed by GluFru (-1.399 ± 0.050), GluGal (-1.317 ± 0.092), and Glu (-0.974 ± 0.038) ($p < 0.05$). The aftertaste-B values was lower in GluXyl than in Glu. These results suggested that binary reducing-sugar systems might reduce lingering bitterness- or astringency-associated responses relative to glucose alone.

The umami response was clearly enhanced in the binary sugar formulations. GluXyl showed the highest umami value, followed by GluFru ($p < 0.05$). This enhancement may be associated with increased levels or improved extractability of water-soluble amino acids, peptides, nucleotides, or Maillard-derived taste-enhancing compounds (Zhang et al., 2023). During fermentation and baking, yeast metabolism and thermal reactions can release or transform amino acids and peptides, while reducing sugars can further react with amino compounds to generate soluble Maillard intermediates. Therefore, the increased umami response in GluXyl and GluFru may reflect the combined effects of fermentation-derived metabolites, amino acid/peptide transformation, and Maillard reaction products (Zhai et al., 2024). GluXyl showed the highest sweetness response, whereas GluFru showed the lowest value (5.000 ± 0.098) ($p < 0.05$), indicating clear differences in the sweetness related response among formulations. Because residual sugar content, moisture distribution, sugar distribution, and crust microstructure were not measured, the mechanism underlying these differences could not be determined from the present data.

The *E*-tongue results indicate that binary reducing sugar systems reshaped the taste profile of whole-wheat lye breads under identical

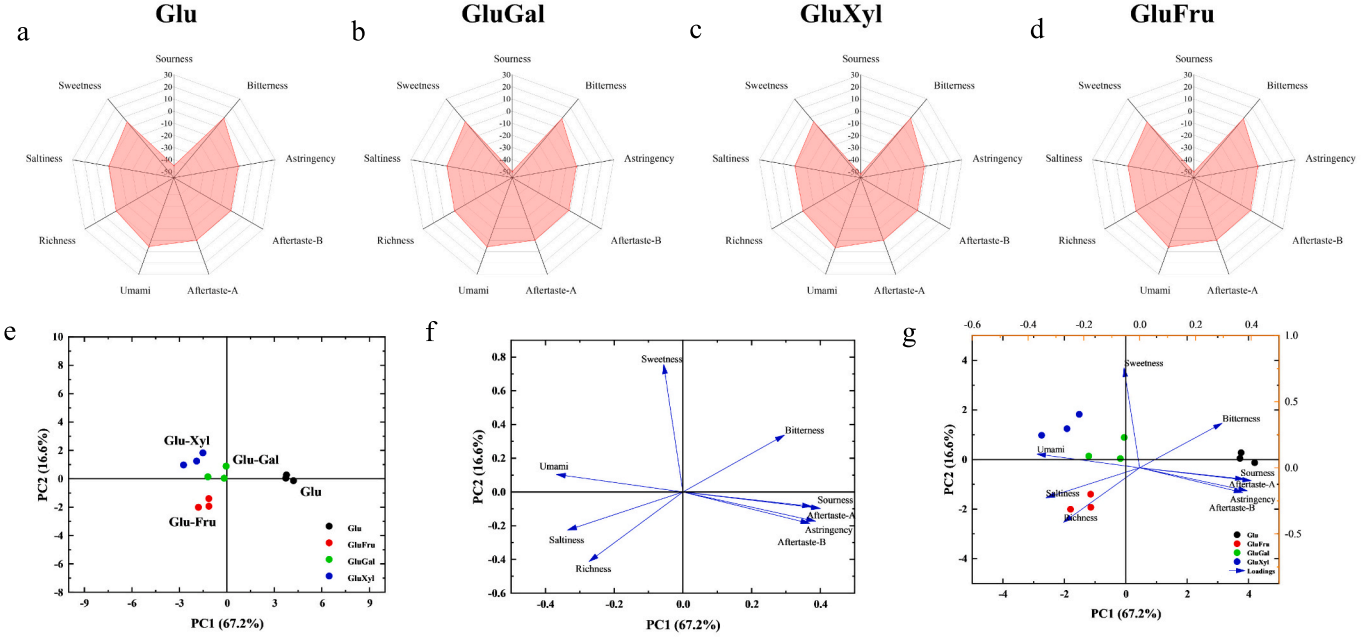

Fig. 3. E-tongue detection results for Glu, GluGal, GluXyl, and GluFru. (a-d): Radar Chart for Glu, GluGal, GluXyl, and GluFru. (e): PCA scores plot. (f): PCA loadings plot. (g): Combined plot of PCA analysis results.

processing conditions. Among the formulations, GluXyl exhibited stronger umami and sweetness responses, lower sourness and astringency responses, and relatively moderate bitterness, suggesting the development of a more complex taste profile following the Maillard reaction. In comparison, the combined E-tongue and E-nose results showed that GluGal exhibited relatively moderate and coordinated responses across both taste and aroma attributes, suggesting a more balanced overall flavor profile. Further integration with untargeted metabolomics is needed to identify the key compounds responsible for these non-volatile flavor differences.

3.5.2. PCA analysis of E-tongue results

The PCA score and loading plots based on E-tongue responses revealed clear differences in the non-volatile taste fingerprints of whole-wheat lye breads prepared with different reducing sugar systems (Fig. 3). PC1 and PC2 explained 67.2% and 16.6% of the total variance, respectively, with a cumulative contribution of 83.8%, indicating that the first two principal components captured the major taste-related variation among the four formulations.

The PCA score plot showed that the Glu formulation was mainly distributed on the positive side of PC1 and was located close to the loading directions of sourness, bitterness, astringency, aftertaste-A, and aftertaste-B. This distribution was consistent with the radar plot results, suggesting that glucose alone produced a taste profile with stronger bitterness-, sourness-, and aftertaste-related responses. GluXyl was clearly separated from Glu along PC1 and was positioned in the negative PC1 and positive PC2 region, close to the directions of umami and sweetness. The PCA pattern suggests that the GluXyl system reshaped the taste profile toward a more umami- and sweetness-associated direction, which may be related to formulation-dependent changes in residual sugars, water-soluble amino acids, small peptides, and Maillard-derived taste-active intermediates (Xiao et al., 2025).

The GluGal samples were located close to the PCA origin, indicating a relatively moderate and balanced taste profile. Compared with GluXyl and GluFru, the GluGal system may have induced less pronounced changes in taste-related compounds, thereby producing a milder non-volatile flavor profile. In thermally processed or fermented foods, differences in flavor are often associated with the synergistic changes of carbohydrates, organic acids, amino acids, and secondary metabolites, rather than depending solely on any single class of compounds (Sheng et al., 2024). This further demonstrates that the Maillard reaction involving GluGal during processing is relatively mild.

The PCA results demonstrated that reducing-sugar composition constituted a key factor reshaping the non-volatile taste fingerprints of whole-wheat lye bread under identical processing conditions.

3.6. Analysis of non-targeted metabolomics results

3.6.1. Quality control and multivariate statistical results

Untargeted metabolomics provides a comprehensive strategy for profiling low-molecular-weight compounds in complex food matrices, enabling the identification of chemical markers associated with food quality, authenticity, and processing-induced compositional changes (Mahanti et al., 2024; Shi et al., 2024). When integrated with chemometrics and pathway analysis, this approach can further reveal the metabolic pathways underlying flavor formation, quality differentiation, and formulation-dependent changes in processed foods (Zhong et al., 2022). Reliable biological interpretation of untargeted metabolomics data requires appropriate quality control procedures, including the injection of pooled QC samples and PCA-based QC clustering, to assess the stability and reproducibility of the analytical dataset (Li, Yuan, et al., 2025).

As shown in Fig. S1, the experimental retention times were highly correlated with the reference retention times, with an R^2 of 0.99 and a regression coefficient of 1.02, indicating good agreement between the experimental and reference values and supporting reliable retention-time correction and alignment. In addition, the QC samples clustered closely in the PCA score plot, suggesting good repeatability among the QC injections.

The PCA model showed that PC1 and PC2 explained 25.8% and 17.3% of the total variance, respectively, with a cumulative contribution of 43.1%. This indicated that the first two principal components captured the major metabolic variation among the four whole-wheat lye bread formulations. The PCA score plot revealed treatment-dependent variation in the non-volatile metabolite profiles of the four whole-wheat lye bread formulations; however, complete separation among the groups was not observed. Glu, GluFru, and GluGal showed partial overlap in the central region of the score plot, although GluGal tended to extend toward positive PC2 values.

3.6.2. Multigroup co-analysis of untargeted metabolomics

A total of 84,272 metabolic features were detected in this study. Based on the annotation criteria specified in Table S3, 4919 metabolites were putatively annotated and further classified into 13 superclasses and 68 classes (Fig. 4(a, b)), indicating the high chemical diversity of the whole-wheat lye bread matrix. The major superclasses included amino acids and derivatives (32.26%), carbohydrates (4.31%), fatty acyls (1.08%), glycerolipids (4.86%), glycerophospholipids (7.46%), lipids (22.87%), organic acids and derivatives (2.87%), others (4.51%), phenylpropanoids (13.82%), prenol lipids (0.10%), sphingolipids (4.15%), steroids and steroid derivatives (1.57%), and sterol lipids (0.14%). These results suggested that amino acid derivatives, lipid-related metabolites, and phenylpropanoids constituted the dominant non-volatile metabolite classes in the bread samples. As shown in Fig. 4c, K-means clustering grouped the differential metabolites into nine clusters according to their standardized intensity profiles across the four formulations. Distinct metabolite response patterns were observed among the reducing sugar systems. In particular, metabolites in clusters 1, 2, 4, 5, 6, and 9 showed increased accumulation in specific binary-sugar formulations, whereas those in clusters 3 and 7 displayed decreasing trends or lower relative intensities. These clustering patterns indicated that the different reducing sugar systems did not uniformly alter the metabolome but instead reshaped specific metabolite groups in a formulation-dependent manner, with GluXyl and GluGal showing more pronounced changes in particular metabolite subsets.

The PCA score plot showed clear metabolic separation among the four formulations, suggesting that reducing sugar composition was a major factor reshaping the non-volatile metabolite profiles of whole-wheat lye breads. PCA of the non-volatile metabolomic dataset showed that PC1 and PC2 accounted for 27.1% and 14.5% of the total variance, respectively, with a cumulative explanatory contribution of 41.6% (Fig. 4d). The score distribution revealed formulation-dependent variation in the metabolite profiles, although complete separation among the four formulations was not observed. Glu samples were mainly distributed in the positive PC2 region, whereas GluGal samples tended to shift toward negative PC2 values. GluFru partially overlapped with both Glu and GluGal, indicating that the metabolic differences among these formulations were not completely resolved by the first two principal components. GluXyl showed relatively greater dispersion in the PCA space, reflecting greater within-group variation. These formulation-dependent differences may be associated with coordinated changes in carbohydrates, amino acids, lipids, and Maillard reaction-related intermediates (Shakoor et al., 2022). Overall, the PCA results suggested that reducing sugar composition contributed to variation in the non-volatile metabolite profiles of whole-wheat lye breads, while subsequent supervised and differential metabolite analyses were required to further resolve formulation-specific metabolic changes.

Partial least squares discriminant analysis (PLS-DA) maximizes inter-group discrimination by incorporating group-label information, making it a useful multivariate tool for identifying metabolite features responsible for sample classification in complex food metabolomic datasets (Gu et al., 2025; Windarsih et al., 2022). The PLS-DA score plot showed that

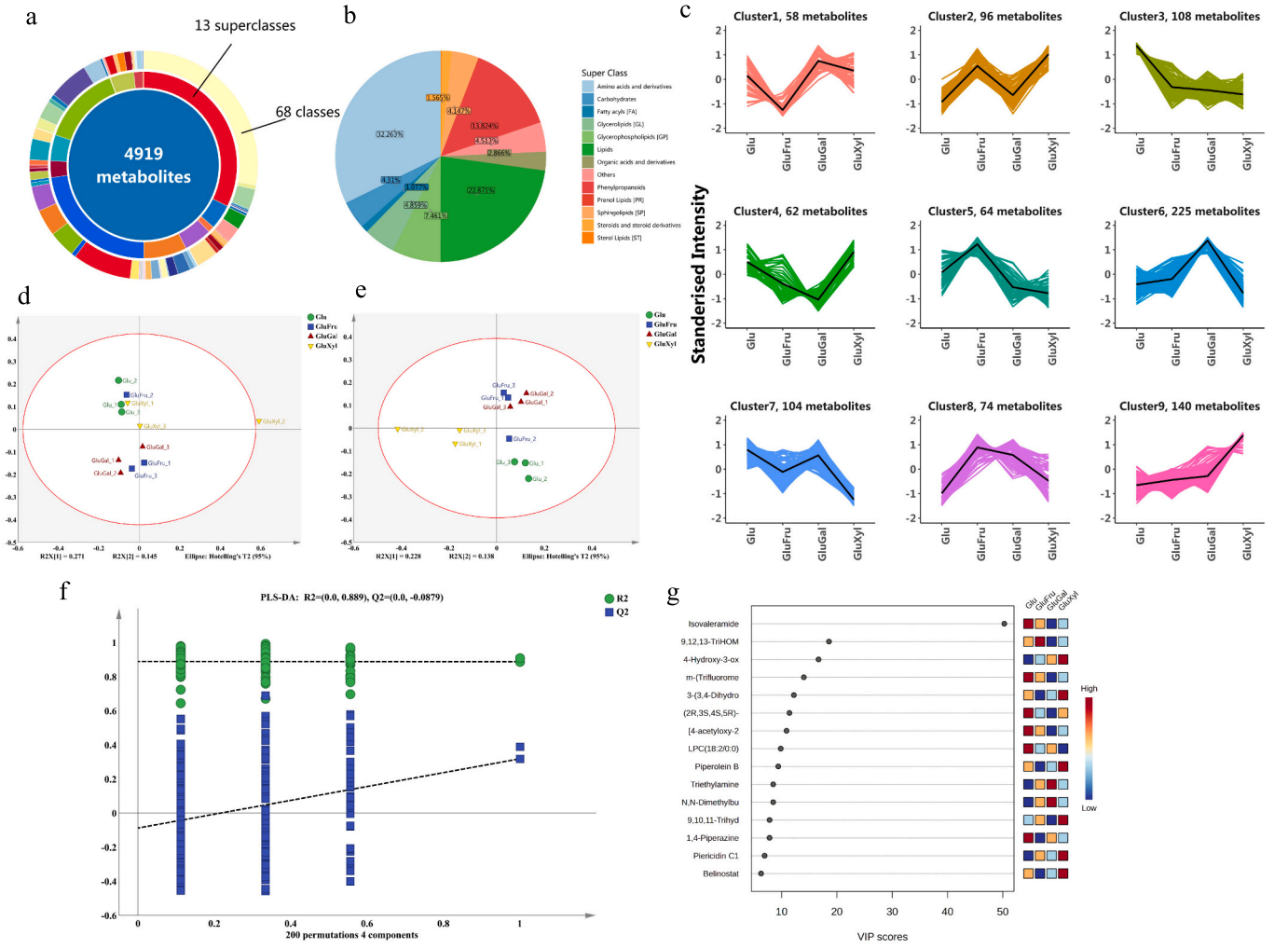

Fig. 4. Results of metabolomic analysis of four types of whole-wheat lye breads. (a): Metabolite classification overview. (b): Pie chart of metabolite super-class distribution. (c): K-means clustering analysis of differential metabolite profiles (nine metabolite clusters). (d): PCA score plot. (e): PLS-DA score plot. (f): Permutation test of the PLS-DA model. (g): VIP score plot of PLS-DA.

component 1 and component 2 explained 22.8% and 13.8% of the total variance, respectively (Fig. 4e). All samples were located within the Hotelling's T^2 95% confidence ellipse, with no extreme score-space outliers observed. The score distribution showed formulation-dependent discrimination, with Glu and GluGal forming relatively compact clusters, whereas GluFru exhibited moderate within-group dispersion. GluXyl showed the most pronounced shift toward the negative direction of component 1, although some within-group variation remained. These results suggested that the reducing sugar composition contributed to systematic differences in the overall metabolite profiles. Based on the global PLS-DA model, 678 metabolite features had VIP values >1, indicating that a large number of variables contributed to the discrimination among the four formulations. The corresponding heatmap further revealed formulation-dependent abundance patterns among these features, with several metabolite subsets showing distinct distributions across the reducing sugar systems (Fig. 4g). Model validation by permutation testing showed a negative Q^2 intercept (−0.0879), indicating that the predictive performance decreased after random permutation of the class labels and supporting the statistical validity of the observed group discrimination (Fig. 4f).

Because the global PLS-DA yielded a large number of VIP > 1 features and did not directly resolve which metabolic changes were specifically associated with each binary reducing sugar formulation, pairwise OPLS-DA was subsequently performed for Glu vs GluFru, Glu vs GluGal, and Glu vs GluXyl. These pairwise models were further combined with fold-change and univariate statistical analyses to prioritize candidate differential metabolites associated with each reducing sugar system.

3.6.3. OPLS-DA analysis results for Glu vs GluFru

As shown in Fig. 5a, the volcano plot revealed 235 up-regulated and 200 down-regulated metabolites (FC > 2 or < 0.5, $p < 0.05$), indicating that the introduction of fructose markedly altered the non-volatile metabolite profile of whole-wheat lye bread. The higher number of up-regulated metabolites suggests that the GluFru formulation promoted the accumulation or retention of a broader range of water-soluble compounds during fermentation, alkaline treatment, and baking. Similar LC-MS based food metabolomics studies have shown that formulation and fermentation conditions can reshape non-volatile metabolites, thereby contributing to food flavor differentiation (Rong et al., 2024).

The OPLS-DA score plot further showed a clear separation between Glu and GluFru along the predictive component, although some within-group dispersion was observed for GluFru (Fig. 5b). All samples remained within the Hotelling's T^2 95% confidence ellipse. The original OPLS-DA model showed high goodness of fit and predictive ability, with $R^2Y = 0.999$ and $Q^2 = 0.76$). In the 200-permutation test, none of the permuted models exceeded the R^2Y or Q^2 values of the original model,

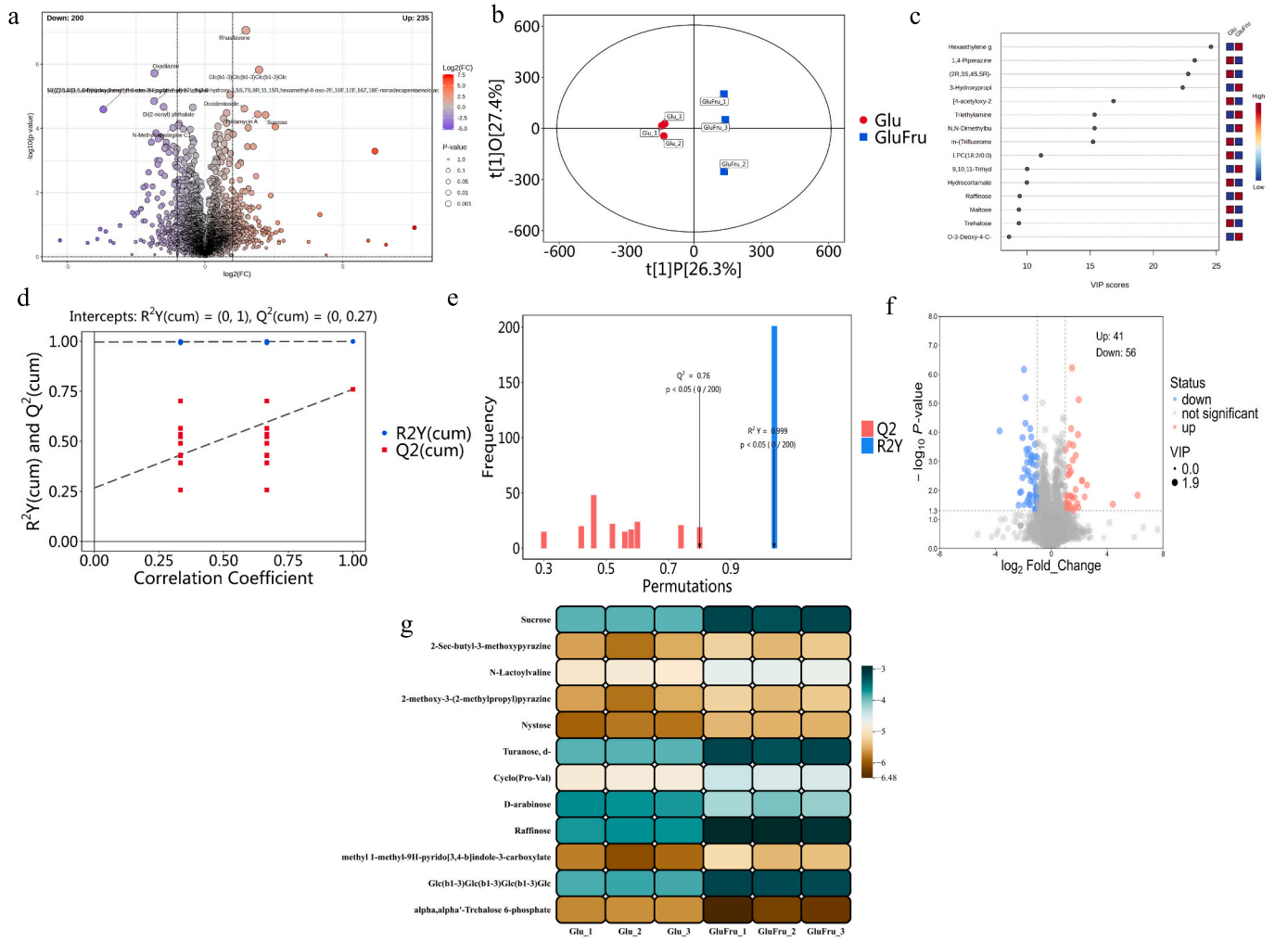

Fig. 5. OPLS-DA analysis results for Glu vs GluFru. (a): Volcano plot. (b): OPLS-DA score plot. (c): VIP plot. (d, e): Permutation test plot for the OPLS-DA model. (f): Volcano plot of metabolites with VIP > 1, FC > 2 or < 0.5, and $p < 0.05$. (g): Heatmap of key differentially expressed metabolites associated with the Maillard reaction.

supporting the statistical relevance of the observed group discrimination (Sheng et al., 2024; Shi et al., 2024). However, the positive Q^2 regression intercept (0.27) indicated that potential model overfitting could not be completely excluded. Therefore, the OPLS-DA results were interpreted cautiously and were not used alone to define differential metabolites. A total of 515 metabolite features showed VIP values >1 and were considered to contribute substantially to the discrimination between Glu and GluFru. To improve the specificity of candidate selection, the multivariate results were subsequently integrated with FC and univariate statistical analyses. Using the combined criteria of VIP > 1, FC > 2 or < 0.5, and $p < 0.05$, 97 key differential metabolites were retained. These metabolites were mainly including 31 amino acids and derivatives, 11 carbohydrates, 17 lipids, 19 phenylpropanoids, 8 sphingolipids, 3 glycerophospholipids, 3 organic acids and derivatives, 2 steroids and steroid derivatives, 1 glycerolipids, and 2 other metabolites. Collectively, these results indicated that fructose addition was associated with coordinated changes across multiple classes of non-volatile metabolites.

Further examination of the 97 key differential metabolites identified a subset of compounds potentially associated with Maillard and related thermal reactions (Fig. 5g). The enrichment of several carbohydrate-related metabolites suggested that fructose addition substantially altered the carbohydrate precursor pool rather than uniformly increasing the abundance of all Maillard substrates (Landberg et al., 2024). In particular, reducing carbohydrates such as D-turanose and reducing-end oligosaccharides may participate directly in amino-arbonyl reactions, whereas sucrose, raffinose, and nystose are more appropriately considered indirect components of the carbohydrate pool (Timmermans et al., 2022). The presence of Glc(β1–3)Glc(β1–3)Glc (β1–3)Glc may reflect β-1,3-glucan-related oligosaccharide turnover, potentially associated with yeast-derived β-glucan, although its precise origin could not be established from the untargeted metabolomic data (Kuo et al., 2025). Yeast-associated carbohydrate metabolism during proofing may also have contributed to changes in the residual sugar pool, particularly through sucrose hydrolysis and subsequent utilization of fermentable sugars. Fructose can generate a broad range of reactive carbonyl compounds, including 3-deoxyglucosone, methylglyoxal, and glyoxal, which serve as important intermediates linking sugar degradation with downstream Maillard reactions (Bolchini et al., 2025; Landberg et al., 2024; Rögner et al., 2021). The higher abundance of the β-carboline-type feature in GluFru was also consistent with previous model studies showing that α-dicarbonyl compounds derived from fructose or glucose can react with tryptophan to generate β-carboline derivatives, with fructose favoring the formation of several such products.

Collectively, these results suggested that fructose addition redirected the low-molecular-weight thermal reaction network toward a distinct carbohydrate- and carbonyl-associated metabolite profile rather than simply increasing the overall extent of the Maillard reaction.

3.6.4. OPLS-DA analysis results for Glu vs GluGal

As shown in Fig. 6a, the volcano plot identified 503 differential metabolic features between Glu and GluGal, including 304 features with higher abundance and 199 with lower abundance in the GluGal group (FC > 2, $p < 0.05$). These results indicated that galactose addition was associated with substantial changes in the non-volatile metabolite profile of whole-wheat lye bread.

The OPLS-DA score plot further showed clear separation between Glu and GluGal along the predictive component, which explained 31.5% of the X-matrix variance, whereas the first orthogonal component accounted for an additional 18.7% (Fig. 6b). All samples were located within the Hotelling's T^2 95% confidence ellipse, with no extreme score-space outliers observed. The original OPLS-DA model showed high goodness of fit and predictive ability, with $R^2Y = 1.000$ and $Q^2 = 0.847$. In the 200-permutation test, none of the permuted models reached the R^2Y or Q^2 values of the original model, supporting the observed discrimination between Glu and GluGal. However, the positive Q^2 regression intercept (0.14) indicated that potential model overfitting could not be completely excluded. Therefore, the supervised OPLS-DA model was interpreted together with univariate FC and significance analyses rather than being used alone to define differential metabolites. A total of 910 metabolite features showed VIP values >1 and were considered to contribute substantially to the discrimination between Glu and GluGal. After integration of the multivariate and univariate analyses, 218 key differential metabolites were retained according to the combined criteria of VIP > 1, FC > 2 or < 0.5, and $p < 0.05$. These metabolites were predominantly assigned to amino acids and their derivatives, lipids, phenylpropanoids, and carbohydrates, together with smaller numbers of metabolites belonging to several other chemical classes. Collectively, these results indicated that galactose addition was associated with broad changes in multiple classes of non-volatile metabolites.

Further examination of the 218 key differential metabolites identified a subset of compounds potentially associated with Maillard and related thermal reactions (Fig. 6g). Most of these metabolites showed higher abundance in GluGal than in Glu, indicating that galactose addition was associated with a distinct pattern of Maillard-related low-molecular-weight compounds. Notably, 2,5-dimethylpyrazine, 2,6-dimethylpyrazine, 2-ethylpyrazine, and 2,3-diethylpyrazine were consistently enriched in GluGal (Zhai et al., 2024). Alkylpyrazines are characteristic Maillard-derived heterocyclic compounds formed through reactions involving sugar-derived α-dicarbonyls and amino-containing intermediates and are commonly associated with roasted and nutty flavor characteristics (Rong et al., 2024). The higher abundance of 2-acetylfuran provided additional evidence of altered sugar-derived thermal chemistry, as furan derivatives can arise from both Maillard-associated carbonyl reactions and direct thermal degradation of reducing carbohydrates (El Hosry et al., 2025; Lee, Kyoung, et al., 2024).

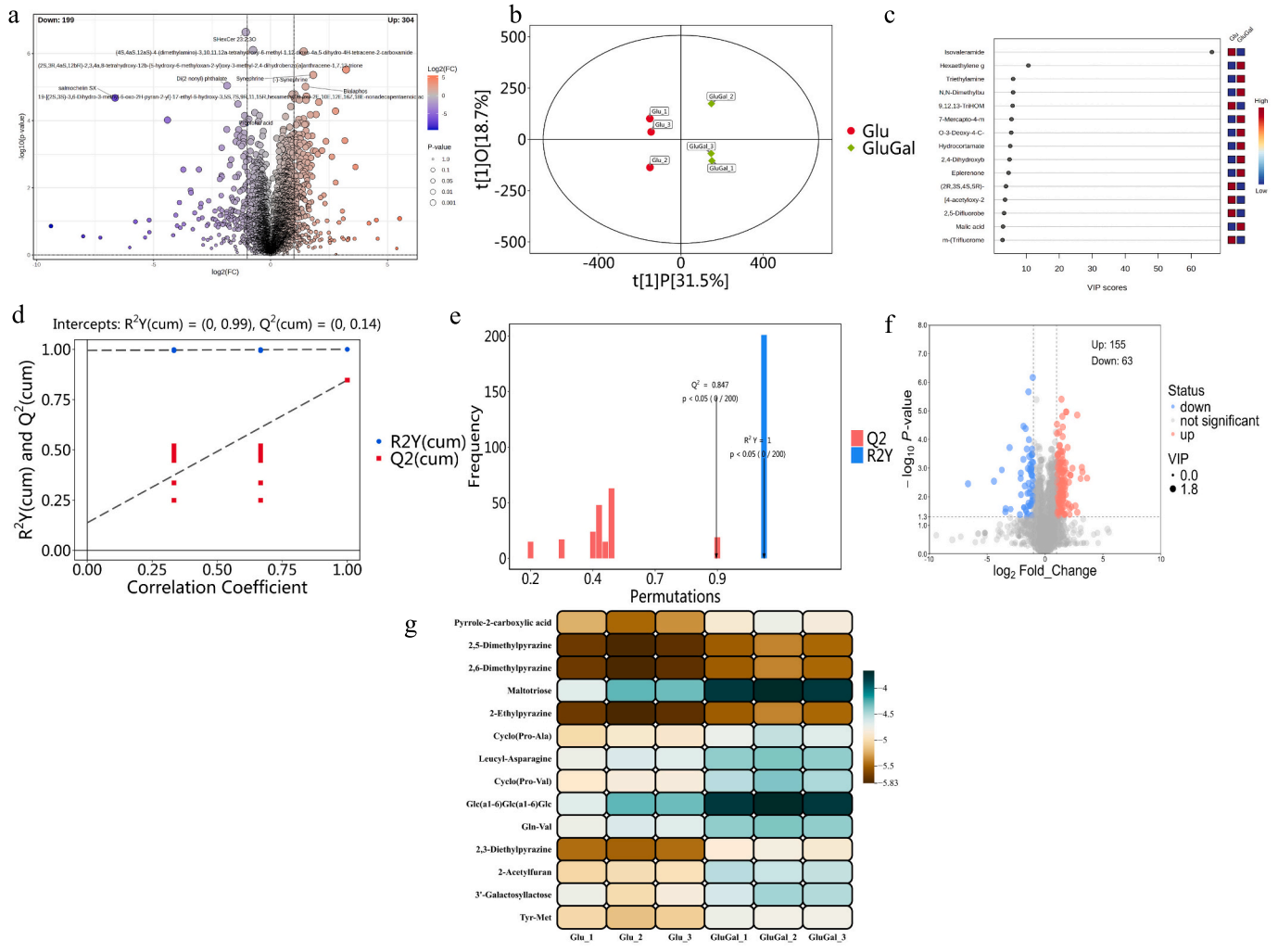

Fig. 6. OPLS-DA analysis results for Glu vs GluGal. (a): Volcano plot. (b): OPLS-DA score plot. (c): VIP plot. (d, e): Permutation test plot for the OPLS-DA model. (f): Volcano plot of metabolites with VIP > 1, FC > 2 or < 0.5, and $p < 0.05$. (g): Heatmap of key differentially expressed metabolites associated with the Maillard reaction.

Several carbohydrate-related metabolites, including maltotriose, Glc (a1–6)Glc(a1–6)Glc, and 3′-galactosyllactose, were also more abundant in GluGal. Because these oligosaccharides possess reducing ends, they may represent components of the residual carbohydrate pool capable of participating in subsequent amino-carbonyl reactions (Murayama et al., 2021; Theng et al., 2024). In parallel, the higher abundance of Leucyl-Asparagine, Gln-Val, and Tyr-Met indicated differences in the pool of amino-containing precursors potentially available for thermal reactions. Cyclo(Pro-Ala) and Cyclo(Pro-Val) were also enriched in GluGal; however, these diketopiperazines are more appropriately regarded as heat-derived peptide cyclization products rather than specific Maillard reaction products. Collectively, the concurrent enrichment of reducing carbohydrate precursors and characteristic pyrazine- and furan-related compounds suggested that galactose addition selectively favored the formation and accumulation of low-molecular-weight Maillard-associated flavor compounds rather than uniformly increasing the overall extent of the Maillard reaction.

3.6.5. *OPLS-DA analysis results for Glu vs GluXyl*

As shown in Fig. 7a, the volcano plot identified 580 differential metabolic features between Glu and GluXyl, including 333 features with higher abundance and 247 with lower abundance in the GluXyl group (FC > 2 or < 0.5, $p < 0.05$). These results indicated that xylose addition was associated with substantial changes in the non-volatile metabolite profile of whole-wheat lye bread.

The OPLS-DA score plot further showed clear separation between Glu and GluXyl along the predictive component, which explained 27.2% of the X-matrix variance, while the first orthogonal component accounted for an additional 35.1% (Fig. 7b). All samples were located within the Hotelling's T^2 95% confidence ellipse. The original OPLS-DA model showed high goodness of fit and predictive ability, with $R^2Y = 0.998$ and $Q^2 = 0.764$. In the 200-permutation test, none of the permuted models reached the R^2Y or Q^2 values of the original model, supporting the observed discrimination between Glu and GluXyl. However, the positive Q^2 regression intercept (0.13) indicated that potential model overfitting could not be completely excluded. Therefore, the supervised OPLS-DA results were interpreted together with univariate FC and significance analyses rather than being used alone to define differential metabolites. A total of 463 metabolite features showed VIP values >1 and were considered to contribute substantially to the discrimination between Glu and GluXyl. After integration of the multivariate and univariate analyses, 172 candidate differential metabolites were retained according to the combined criteria of VIP > 1, FC > 2 or < 0.5, and $p < 0.05$. These included 70 amino acids and derivatives, 35 phenylpropanoids, 24 lipids, 11 carbohydrates, 9 sphingolipids, 6 organic acids and derivatives, 4 glycerolipids, 3 glycerophospholipids, 3 steroids and steroid derivatives, 1 fatty acyl, and 6 metabolites assigned to other classes. Only a limited subset of these metabolites could be

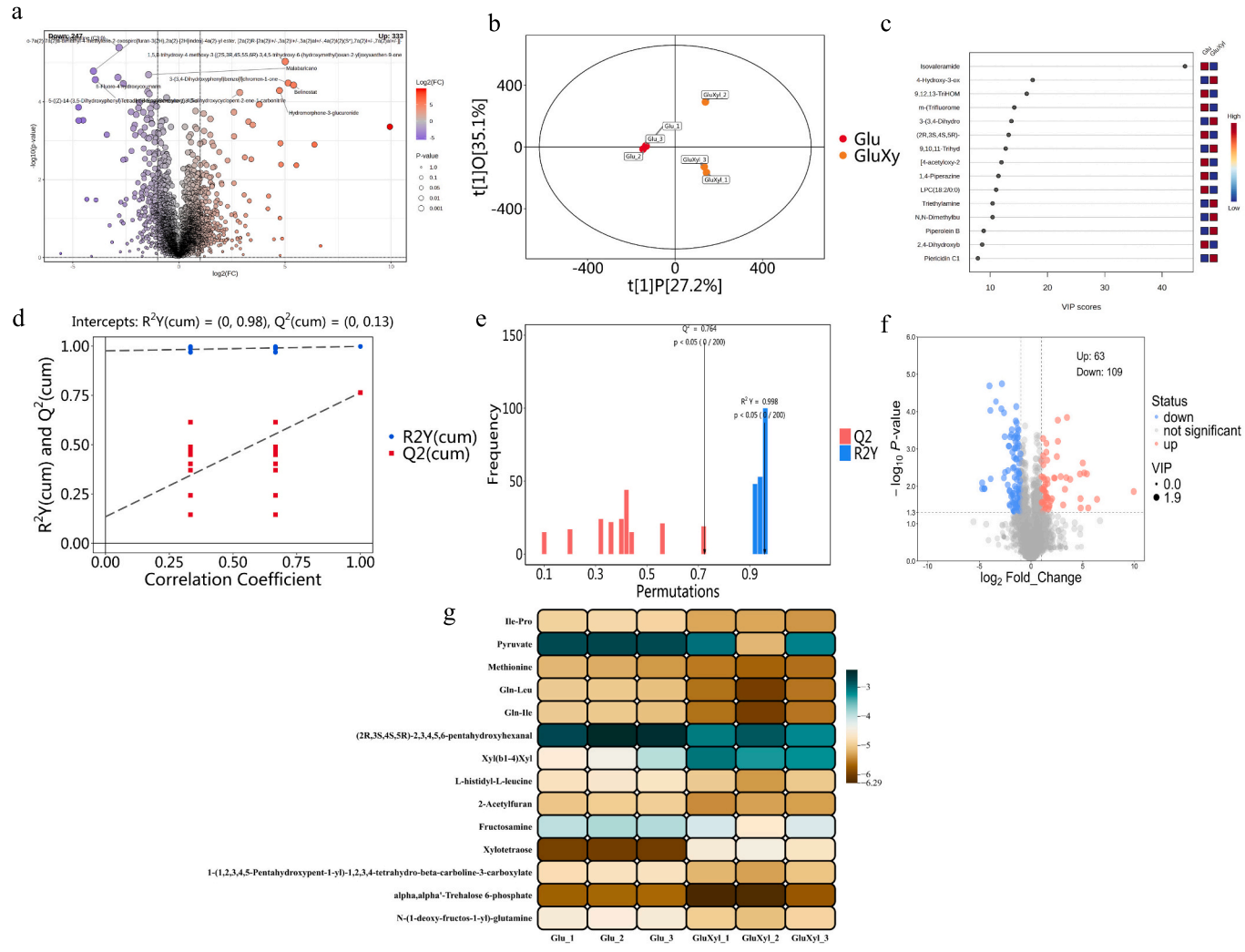

Fig. 7. OPLS-DA analysis results for Glu vs GluXyl. (a): Volcano plot. (b): OPLS-DA score plot. (c): VIP plot. (d, e): Permutation test plot for the OPLS-DA model. (f): Volcano plot of metabolites with VIP > 1, FC > 2 or < 0.5, and $p < 0.05$. (g): Heatmap of key differentially expressed metabolites associated with the Maillard reaction.

plausibly associated with Maillard and related thermal reactions. The broader metabolic differences likely reflected the combined effects of yeast-mediated dough fermentation, endogenous enzymatic transformations, alkaline treatment, lipid oxidation, and thermal processing, rather than changes attributable to the Maillard reaction alone (Murayama et al., 2021).

In contrast to the GluFru and GluGal systems, the GluXyl formulation showed a distinct pattern characterized by higher abundances of xylose-related oligosaccharides, including Xyl(b1–4)Xyl and xylotetraose, together with lower abundances of several amino acid- and peptide-related metabolites. Because amino acids and small peptides can serve as amino donors in amino–carbonyl reactions, their lower residual abundance in GluXyl was consistent with greater precursor utilization, although direct consumption through the Maillard reaction could not be established from endpoint metabolomic data alone. Previous kinetic studies have shown that xylose exhibits higher relative Maillard reactivity than glucose and can accelerate the conversion of both sugar and amino substrates in model systems (El Hosry et al., 2025). Several glucose-associated Maillard intermediates and products, including fructosamine and N-(1-deoxy-fructos-1-yl)-glutamine, also showed lower abundance in GluXyl. Fructosamine and fructosyl-amino acids are characteristic Amadori-type products, whereas the detected tetrahydro-β-carboline has been associated with the condensation of glucose and tryptophan (Palomino-Vasco et al., 2023). Their lower abundance therefore did not necessarily indicate a weaker Maillard reaction in GluXyl, but rather suggested reduced accumulation of glucose-derived early intermediates and a shift toward xylose-dependent reaction pathways and/or more rapid downstream conversion. Similarly, the lower abundance of 2-acetylfuran should be interpreted as a difference in furan-product distribution rather than as evidence of reduced overall Maillard activity, because xylose degradation preferentially generates different furanic products, including furfural (Lin et al., 2022). Taken together with the higher melanoidin level observed in GluXyl, these metabolomic patterns were consistent with a more advanced progression of the Maillard reaction in the xylose-containing system. The simultaneous reduction in several low-molecular-weight precursors and glucose-derived intermediates, together with greater formation of late-stage browning products, suggested more rapid intermediate turnover and downstream conversion in GluXyl.

3.6.6. *Summary of metabolomic findings and study limitations*

Fig. 8 summarized the abundance patterns of 37 metabolites potentially associated with Maillard and related thermal reactions across Glu, GluFru, GluGal, and GluXyl, together with a Venn diagram illustrating their overlap among the three pairwise comparisons (Fig. 8 (a, b)). Overall, the three OPLS-DA comparisons revealed distinct sugar-dependent metabolic responses rather than a uniform enhancement of the Maillard reaction. GluFru was characterized primarily by changes in low-molecular-weight carbohydrate- and carbonyl-associated metabolites, whereas GluGal showed greater accumulation of characteristic Maillard-associated heterocyclic flavor compounds, particularly alkylpyrazines and furan derivatives. In contrast, the metabolic pattern of GluXyl, together with its higher melanoidin level, was consistent with greater precursor utilization, more rapid intermediate turnover, and further progression toward late-stage Maillard products. These contrasting profiles suggested that fructose, galactose, and xylose differentially modulated the distribution and progression of Maillard-associated reactions.

Several limitations should be acknowledged. Given the exploratory nature of the untargeted metabolomics and the relatively small sample size, FDR correction was not used for candidate screening, as it could substantially reduce sensitivity in this high-dimensional dataset. Instead, differential metabolites were prioritized using combined VIP, FC, and nominal *p*-value criteria and were therefore interpreted cautiously as candidate features rather than confirmed biomarkers. In addition, metabolite annotations were not systematically verified using authentic standards, and endpoint abundances could not directly establish reaction fluxes. Future work will integrate volatile aroma profiling and targeted metabolomics of key Maillard-related compounds to further validate and strengthen the present findings.

4. Conclusion

As a whole-grain bakery product, whole-wheat lye bread has nutritional advantages but often suffers from limited flavor quality. Regulation of the Maillard reaction through reducing sugar selection provides a feasible strategy for improving its flavor profile. The sensory evaluation and physicochemical analyses indicated that the GluXyl formulation underwent a relatively stronger Maillard reaction than the other reducing sugar systems. The *E*-nose results showed that whole-wheat lye bread prepared with GluXyl was characterized by stronger responses from sensors associated with Maillard-derived volatile fingerprints, particularly W1W, W5S, and W1S, whereas the GluFru sample was more closely related to oxygen-containing volatile signals. The E-tongue

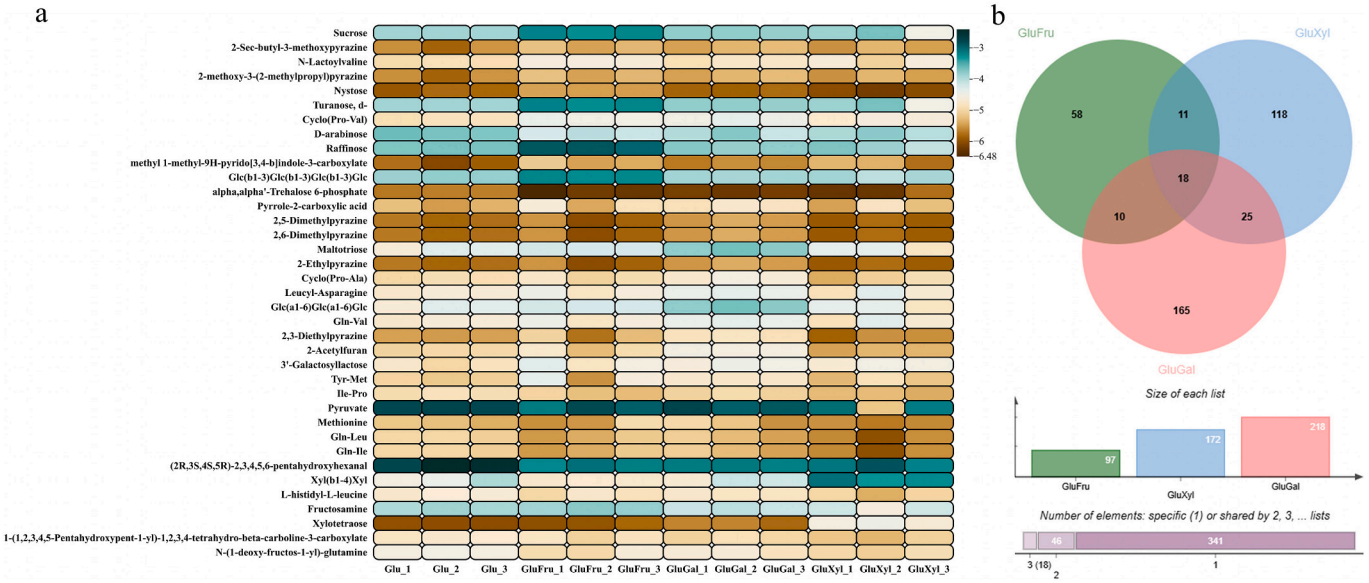

Fig. 8. Analysis of differential metabolites associated with the Maillard reaction. (a): Heatmap. (b): Venn plot.

analysis further showed that GluXyl exhibited stronger umami and sweetness responses, weaker sourness and astringency responses. GluGal exhibited relatively moderate and coordinated responses across both taste and aroma attributes, suggesting a more balanced overall flavor profile. Untargeted metabolomics further revealed distinct sugar-dependent metabolic responses among the binary reducing sugar systems. GluXyl showed a metabolic pattern consistent with greater precursor utilization, enhanced Maillard reaction progression, whereas GluGal favored the accumulation of characteristic Maillard-associated flavor compounds, particularly alkylpyrazines and furan derivatives, and exhibited a more balanced overall flavor profile. These findings indicated that xylose and galactose provided complementary advantages in regulating Maillard reaction progression and flavor formation in whole-wheat lye bread. Future work combining volatile profiling and targeted quantification of key Maillard compounds is needed to validate these sugar-dependent pathways and their sensory contributions.

CRediT authorship contribution statement

Jian Ma: Writing – original draft, Data curation, Conceptualization. **Tuanjie Li:** Methodology, Conceptualization. **Rui Cao:** Software, Investigation, Data curation. **Hui Zhao:** Validation, Supervision, Funding acquisition. **Xuejie Li:** Writing – review & editing, Methodology, Conceptualization. **Jing Lu:** Supervision, Methodology. **Lin Zhao:** Methodology, Investigation, Conceptualization. **Jian Li:** Supervision, Resources, Project administration, Conceptualization.

Declaration of competing interest

The authors declare that they have no known competing financial interests or personal relationships that could have appeared to influence the work reported in this paper.

Acknowledgments

This work was supported by the Key Research and Development Program of Henan Province, China (Grant No. 251111110600).

Appendix A. Supplementary data

Supplementary data to this article can be found online at https://doi.org/10.1016/j.fochx.2026.104800.

Data availability

Data will be made available on request. The raw untargeted LC-MS metabolomics data in this study were deposited in OMIX (Open Archive for Miscellaneous Data), China National Center for Bioinformation, under accession number OMI022334. The dataset is publicly available at https://ngdc.cncb.ac.cn/omix.

References

Bolchini, S., Angeli, L., Ferrentino, G., Van Boekel, M., Amorati, R., Scampicchio, M., & Morozova, K. (2025). Free radical scavenging kinetics of Maillard reaction products: A glucose-glycine model system. *LWT - Food Science and Technology, 217*, Article 117316. https://doi.org/10.1016/j.lwt.2024.117316

Chekima, K., Wong, B., Noor, M. I., Ooi, Y., Yan, S. W., & Chekima, B. (2022). Use of a continuous glucose monitor to determine the glycaemic index of rice-based mixed meals, their effect on a 24 h glucose profile and its influence on overweight and obese young adults' meal preferences. *Foods, 11*(7), Article 983. https://doi.org/10.3390/foods11070983

Cheng, W., Wang, X., Zhang, Z., Ma, L., Liu, G., Wang, Q., … Cheng, K. W. (2021). Development of an isotope dilution UHPLC-QqQ-MS/MS-based method for simultaneous determination of typical advanced glycation end products and acrylamide in baked and fried foods. *Journal of Agricultural and Food Chemistry, 69*(8), 2611–2618. https://doi.org/10.1021/acs.jafc.0c07575

Cong, W., Schwartz, E., Tello, E., Simons, C. T., & Peterson, D. G. (2021). Identification of non-volatile compounds that negatively impact whole wheat bread flavor liking. *Food Chemistry, 364*, Article 130362. https://doi.org/10.1016/j.foodchem.2021.130362

Ding, X. L., Yue, M. X., Gu, H. H., Li, S. Y., Chen, S. Y., Wang, L., & Sun, L. (2024). Effects of wickerhamomyces anomalus co-fermented with *Saccharomyces cerevisiae* on volatile flavor profiles during steamed bread making using electronic nose and HS-SPME-GC-MS. *Foods, 13*(16), Article 2490. https://doi.org/10.3390/foods13162490

Dos Santos Rocha, C., Magnani, M., Jensen Klososki, S., Aparecida Marcolino, V., Dos Santos Lima, M., Queiroz De Freitas, M., Carla Feihrmann, A., Eduardo Barao, C., & Colombo Pimentel, T. (2023). High-intensity ultrasound influences the probiotic fermentation of baru almond beverages and impacts the bioaccessibility of phenolics and fatty acids, sensory properties, and in vitro biological activity. *Food Research International, 173*(2), Article 113372. https://doi.org/10.1016/j.foodres.2023.113372

Du, H. X., Wang, X. P., Yang, H. G., Zhu, F., Cheng, J. R., Peng, X. X., … Liu, X. M. (2023). Effects of mulberry pomace polysaccharide addition before fermentation on quality characteristics of yogurt. *Food Control, 153*, Article 109900. https://doi.org/10.1016/j.foodcont.2023.109900

El Hosry, L., Elias, V., Chamoun, V., Halawi, M., Cayot, P., Nehme, A., & Bou-Maroun, E. (2025). Maillard reaction: Mechanism, influencing parameters, advantages, disadvantages, and food industrial applications: A review. *Foods, 14*(11), Article 1881. https://doi.org/10.3390/foods14111881

Gancarz, M., Malaga-Tobola, U., Oniszczuk, A., Tabor, S., Oniszczuk, T., Gawrysiak-Witulska, M., & Rusinek, R. (2021). Detection and measurement of aroma compounds with the electronic nose and a novel method for MOS sensor signal analysis during the wheat bread making process. *Food and Bioproducts Processing, 127*, 90–98. https://doi.org/10.1016/j.fbp.2021.02.011

Giovanelli, G., & Cappa, C. (2021). 5-hydroxymethylfurfural formation in bread as a function of heat treatment intensity: Correlations with browning indices. *Foods, 10*(2), Article 417. https://doi.org/10.3390/foods10020417

Gu, Z. X., Rao, J. J., & Chen, B. C. (2025). Application of flavoromics approach to evaluate aroma characteristics in malts: Current trends and future outlooks. *Trends in Food Science & Technology, 156*, Article 104878. https://doi.org/10.1016/j.tifs.2025.104878

Hernandez-Aguilar, C., Dominguez-Pacheco, A., Valderrama-Bravo, C., Cruz-Orea, A., Ortiz, E. M., Ivanov, R., & Ordonez-Miranda, J. (2021). Photoacoustic characterization of wheat bread mixed with *Moringa oleifera*. *Current Research in Food Science, 4*, 521–531. https://doi.org/10.1016/j.crfs.2021.07.008

Jost, T., Henning, C., Heymann, T., & Glomb, M. A. (2021). Comprehensive analyses of carbohydrates, 1,2-dicarbonyl compounds, and advanced glycation end products in industrial bread making. *Journal of Agricultural and Food Chemistry, 69*(12), 3720–3731. https://doi.org/10.1021/acs.jafc.0c07614

Jozinović, A., Šarkanj, B., Ačkar, D., Balentić, J. P., Subarić, D., Cvetković, T., … Babić, J. (2019). Simultaneous determination of acrylamide and hydroxymethylfurfural in extruded products by LC-MS/MS method. *Molecules, 24*(10), Article 1971. https://doi.org/10.3390/molecules24101971

Kaufmann, M., Schwarz, K. J., Dallmann, A., Kuballa, T., & Bergmann, M. (2022). 1H NMR spectroscopic discrimination of different beer styles combined with a chemical shift-based quantification approach. *European Food Research and Technology, 248*(3), 635–645. https://doi.org/10.1007/s00217-021-03914-8

Kuo, S., Lin, C., Chang, H., Wang, R., Lin, P., Lu, T., & Lo, Y. (2025). Structural analysis of laminarin-derived oligosaccharides produced by transglycosylation of exo-β-1,3-glucanase ScEXG1from *Saccharomyces cerevisiae*. *Journal of Agricultural and Food Chemistry, 74*(1), 1053–1062. https://doi.org/10.1021/acs.jafc.5c04471

Landberg, R., Karra, P., Hoobler, R., Loftfield, E., Huybrechts, I., Rattner, J. I., … Scalbert, A. (2024). Dietary biomarkers—An update on their validity and applicability in epidemiological studies. *Nutrition Reviews, 82*(9), 1260–1280. https://doi.org/10.1093/nutrit/nuad119

Lee, J., Roux, S., Descharles, D., Rega, B., & Bonazzi, C. (2024). Unravelling caramelization and Maillard reactions in glucose and glucose plus leucine model cakes: Formation and degradation kinetics of volatile markers extracted during baking. *Food Research International, 183*, Article 114183. https://doi.org/10.1016/j.foodres.2024.114183

Lee, J. J., Kyoung, H., Cho, J. H., Park, K. I., Kim, Y., Ahn, J., … Song, M. H. (2024). Change in the gut microbiota of lactating sows and their piglets by inclusion of-dried plasma in sow diets. *Journal of Microbiology and Biotechnology, 34*(3), 516–524. https://doi.org/10.4014/jmb.2311.11001

Li, J. L., Yuan, L. P., Weng, L. L., Yu, C. W., Hu, M. M., Peng, B., & Tu, Z. C. (2025). Integration of lipidomics and flavoromics reveals the lipid-flavor transformation mechanism of fish oil from silver carp visceral with different enzymatic hydrolysis. *Food Chemistry, 477*, Article 143507. https://doi.org/10.1016/j.foodchem.2025.143507

Li, J. X., Qin, F. P., Chen, M. T., Liu, Y. Y., Guo, X. N., Zhu, K. X., … Xing, J. J. (2025). Elucidating flavor compounds in Chinese steamed bread via glutinous rice wine-fermented dough technique: A triangulated analysis combining electronic tongue, SPME-GC-MS, and quantitative descriptive analysis. *Food Bioscience, 73*, Article 107694. https://doi.org/10.1016/j.fbio.2025.107694

Lin, X., Zhang, Q., Qin, Y., Zhong, Q., Lv, D., Wu, X., Fu, P., & Lin, H. (2022). Potential misidentification of natural isomers and mass-analogs of modified nucleosides by liquid chromatography–triple quadrupole mass spectrometry. *Genes, 13*(5), Article 878. https://doi.org/10.3390/genes13050878

Mahanti, N. K., Shivashankar, S., Chhetri, K. B., Kumar, A., Rao, B. B., Aravind, J., & Swami, D. V. (2024). Enhancing food authentication through e-nose and e-tongue technologies: Current trends and future directions. *Trends in Food Science & Technology, 150*, Article 104574. https://doi.org/10.1016/j.tifs.2024.104574

Murayama, D., Rankin, S. A., & Ikeda, S. (2021). Effect of surfactant-induced competitive displacement of whey protein conjugated to acid- or alkali-extracted potato pectin

on emulsion stability. *Food Hydrocolloids, 114*, Article 106558. https://doi.org/10.1016/j.foodhyd.2020.106558

Palomino-Vasco, M., Rodríguez-Cáceres, M. I., & Mora-Díez, N. (2023). Discrimination based on commercial/craft origin and on lager/ale fermentation of undiluted Spanish beer samples: Front-face excitation-emission matrices and chemometrics. *Journal of Food Composition and Analysis, 115*, Article 104946. https://doi.org/10.1016/j.jfca.2022.104946

Pham, T., Tello, E., & Peterson, D. G. (2025). Identification of compounds that contribute to aroma liking of whole wheat bread. *Food Research International, 209*, Article 116192. https://doi.org/10.1016/j.foodres.2025.116192

Rögner, N. S., Mall, V., & Steinhaus, M. (2021). Impact of malt extract addition on odorants in wheat bread crust and crumb. *Journal of Agricultural and Food Chemistry, 69*(45), 13586–13595. https://doi.org/10.1021/acs.jafc.1c05638

Rong, P. X., He, X. Q., Ayyash, M., Liu, Y., Wu, D. T., Geng, F., … Gan, R. Y. (2024). Untargeted metabolomics analysis of non-volatile metabolites and dynamic changes of antioxidant capacity in Douchi with edible mushroom by-products. *Food Chemistry, 431*, Article 137066. https://doi.org/10.1016/j.foodchem.2023.137066

Sawettanun, S., Inukai, R., Yoshihara, A., & Ogawa, M. (2023). Influence of rare sugar syrup on quality attributes and acceptability of bread. *International Journal of Food Science and Technology, 58*(7), 3693–3706. https://doi.org/10.1111/ijfs.16472

Shakoor, A., Zhang, C. P., Xie, J. C., & Yang, X. L. (2022). Maillard reaction chemistry in formation of critical intermediates and flavour compounds and their antioxidant properties. *Food Chemistry, 393*, Article 133416. https://doi.org/10.1016/j.foodchem.2022.133416

Shang, Y. F., Ding, B. M., Ni, Z. J., Thakur, K., Zhang, J. G., & Wei, Z. J. (2025). The flavour substances and key precursor peptides of meaty flavour prepared from Maillard reaction products of *Lycium barbarum* seed meal. *Food Chemistry, 487*, Article 144734. https://doi.org/10.1016/j.foodchem.2025.144734

Sheng, C., Lu, M., Zhang, J., Zhao, W., Jiang, Y., Li, T., Wang, Y., & Ning, J. (2024). Metabolomics and electronic-tongue analysis reveal differences in color and taste quality of large-leaf yellow tea under different roasting methods. *Food Chemistry: X, 23*, Article 101721. https://doi.org/10.1016/j.fochx.2024.101721

Shi, J. C., Liu, Y. F., & Xu, Y. J. (2024). MS based foodomics: An edge tool integrated metabolomics and proteomics for food science. *Food Chemistry, 446*, Article 138852. https://doi.org/10.1016/j.foodchem.2024.138852

Sun, J., AL-Ansi, W., Zhu, F., Fan, M. C., Li, Y., Qian, H. F., & Wang, L. (2023). A novel kneading method for improving the quality of whole wheat dough and bread. *Journal of Cereal Science, 112*, Article 103690. https://doi.org/10.1016/j.jcs.2023.103690

Theng, A. H. P., Osen, R., & Chiang, J. H. (2024). Influence of reducing sugars and protein-to-sugar ratios on volatile profile, pH, and browning intensity of Maillard-reacted nutritional yeast hydrolysate. *International Journal of Food Science and Technology, 59*(9), 6325–6339. https://doi.org/10.1111/ijfs.17373

Timmermans, E., Bautil, A., Brijs, K., Scheirlinck, I., Van der Meulen, R., & Courtin, C. M. (2022). Sugar levels determine fermentation dynamics during yeast pastry making and its impact on dough and product characteristics. *Foods, 11*(10), Article 1388. https://doi.org/10.3390/foods11101388

Wang, Z. J., Wang, W. H., Xu, S., Ding, J., Zeng, X. F., Liu, H., & Wang, F. L. (2023). Diets enriched with finely ground wheat bran alter digesta passage rate and composition of the gut microbiome in sows. *Animal Nutrition, 12*, 32–41. https://doi.org/10.1016/j.aninu.2022.08.012

Windarsih, A., Warmiko, H. D., Indrianingsih, A. W., Rohman, A., Ulumuddin, Y. I., & Suratno, Y. I. (2022). Untargeted metabolomics and proteomics approach using liquid chromatography-orbitrap high resolution mass spectrometry to detect pork adulteration in *Pangasius hypopthalmus* meat. *Food Chemistry, 386*, Article 132856. https://doi.org/10.1016/j.foodchem.2022.132856

Wu, T. F., Deng, C., Luo, S. J., Liu, C. M., & Hu, X. T. (2023). Effect of rice bran on properties of yogurt: Comparison between addition of bran before fermentation and after fermentation. *Food Hydrocolloids, 135*, Article 108122. https://doi.org/10.1016/j.foodhyd.2022.108122

Xiao, Z. R., Wu, S., Liang, H. S., Li, B., & Li, J. (2025). Effects of oligosaccharides, sodium carboxymethyl cellulose and D-allulose as a compound improver on the quality of sugar-reduced bread. *Journal of the Science of Food and Agriculture, 105*(5), 3024–3035. https://doi.org/10.1002/jsfa.14065

Yang, J., Zhang, Y. Q., Chen, P. W., Zeng, X. F., Bai, W. D., Zhang, Y. Y., & Sun, B. G. (2025). Enhancing beef flavor profiles via Maillard reaction of γ-glutamylated beef protein hydrolysates and xylose. *Food Chemistry, 476*, Article 143313. https://doi.org/10.1016/j.foodchem.2025.143313

Yang, S., Fan, W., & Xu, Y. (2019). Melanoidins from Chinese distilled spent grain: Content, preliminary structure, antioxidant, and ACE-inhibitory activities in vitro. *Foods, 8*(10), Article 516. https://doi.org/10.3390/foods8100516

Zhai, H. N., Dong, W. J., Fu, X. F., Li, G. P., & Hu, F. G. (2024). Integration of widely targeted metabolomics and the e-tongue reveals the chemical variation and taste quality of Yunnan arabica coffee prepared using different primary processing methods. *Food Chemistry: X, 22*, Article 101286. https://doi.org/10.1016/j.fochx.2024.101286

Zhang, B. H., Wang, Y., Wang, J. P., Zhang, Y. M., Wang, W., Cao, J. X., … Teng, W. D. (2025). The establishment of ham grade, sensory scores and key flavor substances prediction models for Jinhua ham via e-nose combined with machine learning. *Food Chemistry, 472*, Article 142847. https://doi.org/10.1016/j.foodchem.2025.142847

Zhang, J. A., Zhao, X. C., Li, L. F., Chen, W., Zhao, Q. Z., Su, G. W., & Zhao, M. M. (2023). Application of electronic tongue in umami detection and soy sauce refining process. *Food Chemistry: X, 18*, Article 100652. https://doi.org/10.1016/j.fochx.2023.100652

Zhong, P., Wei, X. Q., Li, X. M., Wei, X. Y., Wu, S. Z., Huang, W. J., … Lei, H. T. (2022). Untargeted metabolomics by liquid chromatography-mass spectrometry for food authentication: A review. *Comprehensive Reviews in Food Science and Food Safety, 21*(3), 2455–2488. https://doi.org/10.1111/1541-4337.12938

Zhu, Y. W., Zhou, X. R., Chen, Y. P., Liu, Z. Y., Jiang, S., Chen, G. L., & Liu, Y. (2022). Exploring the relationships between perceived umami intensity, umami components and electronic tongue responses in food matrices. *Food Chemistry, 368*, Article 130849. https://doi.org/10.1016/j.foodchem.2021.130849